Bioorganic Chemistry 87 (2019) 888–900

Contents lists available at ScienceDirect

Bioorganic Chemistry

journal homepage: www.elsevier.com/locate/bioorg

Synthesis, bioactivity and molecular modeling studies on potential anti-Alzheimer piperidinehydrazide-hydrazones

Sulunay Parlar[a], Gozde Sayar[a], Ayse Hande Tarikogullari[a], Sumru Sozer Karadagli[b], Vildan Alptuzun[a,*], Ercin Erciyas[a], Ulrike Holzgrabe[c]

[a] Department of Pharmaceutical Chemistry, Faculty of Pharmacy, Ege University, 35040 Izmir, Turkey
[b] Department of Pharmaceutical Toxicology, Faculty of Pharmacy, Ege University, 35040 Izmir, Turkey
[c] Institute of Pharmacy and Food Chemistry, University of Wuerzburg, Am Hubland, 97074 Wuerzburg, Germany

ARTICLE INFO

Keywords:
Hydrazone
Acetylcholinesterase/Butyrylcholinesterase inhibitory
Ellman method
Thioflavin T test
Antioxidant activity
Molecular modeling
Synthesis

ABSTRACT

A group of *N*-benzylpiperidine-3/4-carbohydrazide-hydrazones were designed, synthesized and evaluated for acetylcholinesterase (AChE), butyrylcholinesterase (BuChE) activities, $A\beta_{42}$ self-aggregation inhibitory potentials, and antioxidant capacities, *in vitro*. All of the compounds displayed *ee*AChE and *hu*AChE inhibitory activity in a range of IC_{50} = 5.68–11.35 μM and IC_{50} = 8.80–74.40 μM, respectively and most of the compounds exhibited good to moderate inhibitory activity on BuChE enzyme. Kinetic analysis and molecular modeling studies were also performed for the most potent compounds (**1g** and **1j**). Not only the molecular modeling studies but also the kinetic analysis suggested that these compounds might be able to interact with the catalytic active site (CAS) and the peripheral anionic site (PAS) of the enzymes. In the light of the results, compound **1g** and compound **1j** may be suggested as lead compounds for multifunctional therapy of AD.

1. Introduction

Alzheimer's disease (AD) is a progressive, multi-factorial and irreversible neurodegenerative disease associated with permanent memory loss and cognitive dysfunction. Based on World Alzheimer's Report, there are approximately 47 million people suffering from AD and it is estimated to reach up to 131 million by 2050, worldwide [1].

Due to its complex nature, the actual pathophysiology of AD is not completely identified. Several mechanisms have been reported to explain the pathophysiology of AD, including loss of cholinergic neurotransmission [2], deposition of β-amyloid (Aβ) plaques [3], accumulation of hyperphosphorylated tau-protein [4], and increased oxidative stress [5]. In order to combat these pathophysiologic effects, different strategies were suggested. Cholinergic hypothesis is one of the accepted therapeutic approaches for the palliative treatment of AD. According to this hypothesis, decline of cognitive function is related to the decreased concentration of pre-synaptic neurotransmitter acetylcholine (ACh) in the brain. Increasing the ACh levels at synapses by inhibiting AChE enzyme can be an effective way for the treatment of AD [6]. AChE and BuChE, two types of cholinesterase (ChE) enzymes, are both able to catalyze the degradation of ACh. Many studies have shown that while the AChE activity decreases, the BuChE activity increases in AD [7,8]. For this purpose, BuChE inhibitors may also be attractive targets for AD therapy due to the compensatory ability of BuChE over AChE.

Amyloid hypothesis is another strategy developed for the treatment of AD. According to this hypothesis, the deposition of extracellular aggregates of Aβ-peptide that initiates the pathogenic cascade leads to neuronal cell death associated with AD [9]. Thus, inhibiting Aβ aggregation has drawn attention of many researchers in the development of effective therapies. Besides, AChE is known to have a potential role in Aβ-aggregation in Alzheimer patients [10]. AChE enzyme has a deep, narrow hydrophobic gorge with a depth of 20 Å with two main substrate-binding sites; catalytic anionic site (CAS) at the bottom and peripheral anionic site (PAS) at the entrance of the gorge due to X-ray crystallography [11]. Several studies have been reported that molecules interacting with PAS prevent the initiation of Aβ-aggregation whereas the ones interacting with both PAS and CAS which are referred as dual-site inhibitors not only inhibit the AChE enzyme but also block AChE-induced aggregation [10,12]. Thus, dual-binding inhibitors can be more effective agents for the management of AD [13,14].

On the other hand, oxidative stress plays a pivotal role in AD pathogenesis [15] and regarded as another therapeutic strategy for AD treatment [16,17]. Recent studies indicate that decreasing the oxidative stress and increasing the antioxidant protection is an effective way to

* Corresponding author at: Ege University, Faculty of Pharmacy, Department of Pharmaceutical Chemistry, 35040 Bornova, Izmir, Turkey.
E-mail address: vildan.alptuzun@ege.edu.tr (V. Alptuzun).

https://doi.org/10.1016/j.bioorg.2018.11.051
Received 18 August 2018; Received in revised form 13 November 2018; Accepted 27 November 2018
Available online 28 November 2018
0045-2068/

prevent or to reduce the progression of AD [18–20].

Taken together, a combined therapy involving the inhibition of the ChE enzymes, aggregation of Aβ-peptide and oxidative stress may be more effective as a concept of Multi-Target Drug Ligands (MTDLs).

So far, four ChE inhibitors (tacrine, donepezil, galantamine, and rivastigmine) and a *N*-methyl-D-aspartate (NMDA) receptor antagonist (memantine) were approved by FDA. Therefore, many compounds are still been developed to inhibit AChE and BuChE for the treatment of AD [21].

In this study, *N*-benzylpiperidine core was chosen for favorable interactions since the *N*-benzylpiperidine fragment of donepezil has a binding affinity for the active site of AChE and it is known that the protanable nitrogen atom plays a pivotal role in enzyme-ligand interactions [22,23]. On the other hand, an aromatic phenyl ring bearing electron withdrawing or donating substituents was selected as the other terminal moiety on the basis of its potency of hydrophobic and π-π interactions with the aromatic residues. Thus, *N*-benzylpiperidine and the substituted phenyl ring were expected to bind both to the entrance and inside the enzyme gorge of AChE. Also, it is reported that compounds having hydrazide-hydazone functional groups were found to have antioxidant properties [24]. Therefore, *N*-benzylpiperidine and the substituted phenyl ring was linked to hydrazide-hydrazone functional group in order to synthesize a series of compounds to evaluate AChE, BuChE, $A\beta_{42}$ aggregation inhibitory and antioxidant potentials, *in vitro*. Molecular modeling studies were also carried out for the selected compounds to investigate the ligand-enzyme binding interactions and structure-activity relationships of the compounds.

2. Results and discussion

2.1. Chemistry

In this study, 20 piperidinehydrazide-hydrazone derivatives with a benzyl moiety attached from the piperidine nitrogen were synthesized. The synthesis of the final compounds were realized in three steps as illustrated in Scheme 1. Initially, ethyl nipecotate/ethyl isonipecotate and benzyl chloride were stirred in acetonitrile in the presence of triethylamine to yield ethyl 1-benzylpiperidine-3-carboxylate or ethyl 1-benzylpiperidine-4-carboxylate. Then, the obtained intermediate was reacted with hydrazinium hydroxide in ethanol under reflux condition. Finally, the hydrazide intermediate was condensed with various benzaldehydes bearing different electron withdrawing or donating substituents at *para* position to achieve the final compounds.

The structures of the final compounds were confirmed by FT-IR, ^{1}H NMR, ^{13}C NMR, MS and elemental analyses. According to the ^{1}H- and ^{13}C NMR spectra, the aromatic and aliphatic proton signals were

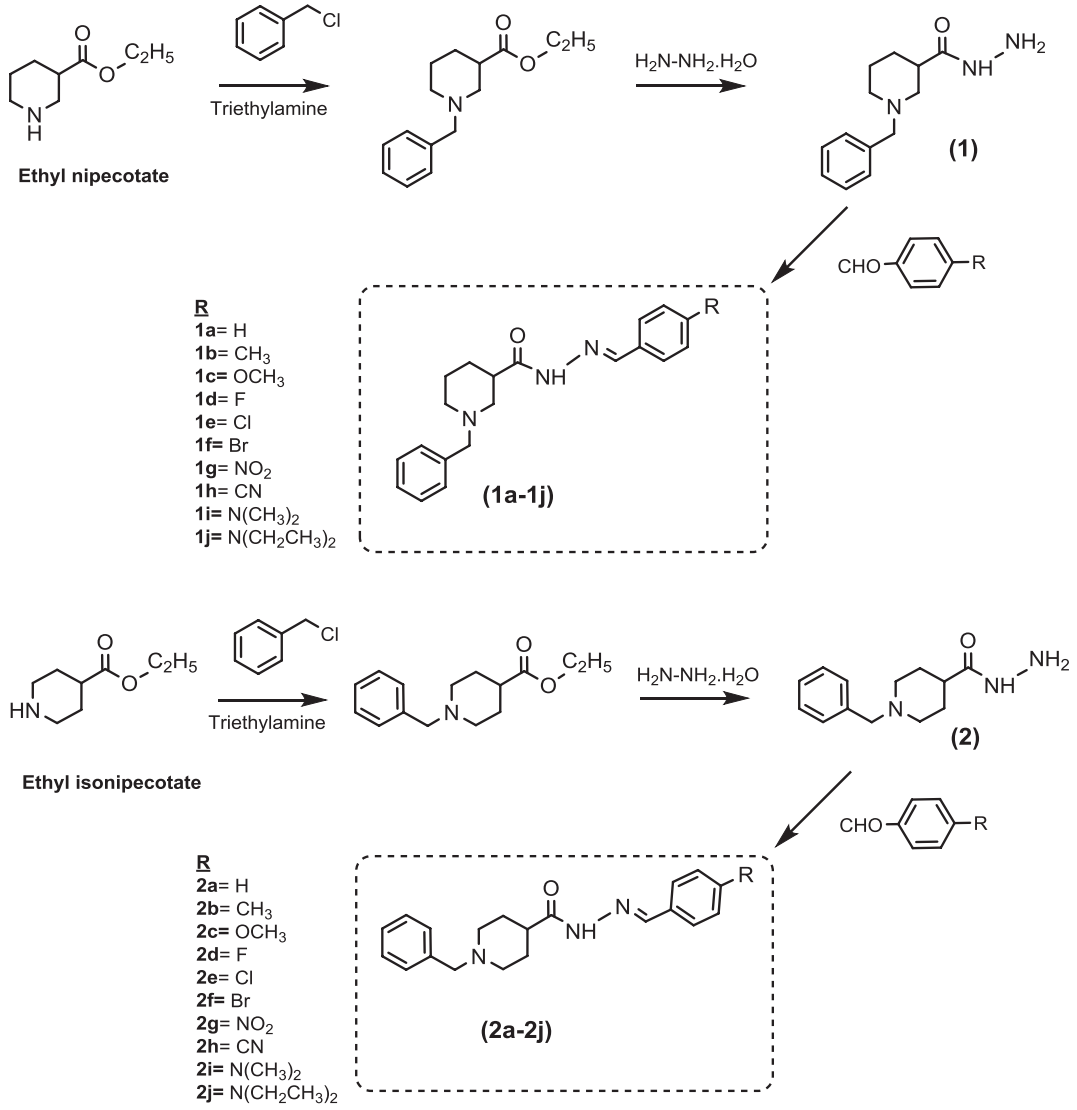

Scheme 1. Synthesis pathway of the final compounds.

Table 1
In vitro AChE, BuChE and Aβ-peptid inhibitory activities of the final compounds.

Compound	IC_{50} ± SEM (μM)[a]		Selectivity AChE/BuChE	% Aβ inhibition	
	*ee*AChE	*eq*BuChE		100 μM ± std	25 μM ± std
1a	6.85 ± 0.17	8.87 ± 0.32	0.77	15.09 ± 0.44	6.16 ± 0.13
1b	10.43 ± 0.14	8.65 ± 0.13	1.20	69.99 ± 0.86	39.79 ± 0.60
1c	7.22 ± 0.26	31.04 ± 0.24	0.23	55.62 ± 0.85	31.99 ± 0.68
1d	7.52 ± 0.47	25.52 ± 0.55	0.29	49.55 ± 0.36	26.89 ± 0.91
1e	6.75 ± 0.25	11.71 ± 2.64	0.58	49.96 ± 0.33	36.48 ± 0.56
1f	7.18 ± 0.26	9.49 ± 0.19	0.82	58.26 ± 0.79	43.70 ± 0.46
1g	5.68 ± 0.48	33.19 ± 2.08	0.17	79.34 ± 1.04	53.18 ± 0.85
1h	6.58 ± 0.75	35.63 ± 0.68	0.18	nd	nd
1i	6.59 ± 0.38	4.54 ± 0.26	1.45	27.63 ± 0.50	8.52 ± 1.35
1j	6.16 ± 0.15	0.81 ± 0.03	8.13	53.18 ± 1.04	46.03 ± 0.99
2a	8.99 ± 0.30	13.53 ± 0.24	0.66	41.66 ± 0.57	14.95 ± 1.02
2b	10.66 ± 0.92	5.10 ± 0.18	2.09	33.21 ± 0.76	18.18 ± 0.64
2c	8.14 ± 1.06	25.63 ± 1.36	0.32	28.36 ± 0.51	3.66 ± 0.37
2d	7.60 ± 0.78	11.43 ± 0.37	0.66	18.58 ± 1.10	8.80 ± 0.51
2e	10.19 ± 0.24	12.96 ± 0.34	0.79	27.24 ± 2.59	11.66 ± 0.27
2f	9.83 ± 0.42	14.21 ± 0.15	0.69	23.36 ± 1.14	7.61 ± 0.98
2g	6.33 ± 0.28	22.19 ± 0.20	0.29	52.54 ± 0.87	22.36 ± 0.83
2h	7.09 ± 0.14	> 50		nd	nd
2i	8.94 ± 0.59	33.4 ± 0.62	0.27	47.95 ± 0.31	15.36 ± 1.10
2j	11.35 ± 0.73	8.20 ± 0.44	1.38	59.98 ± 0.41	40.30 ± 0.20
Tacrine HCl	0.075 ± 0.02	0.0098 ± 0.0002	7.65		
Galantamine	0.43 ± 0.03	14.92 ± 0.57	0.02		
Rivastigmine	10.87 ± 0.24	5.13 ± 0.18	2.12		
Curcumin				98.38 ± 0.03	92.79 ± 0.10

nd: not determined.
[a] Data are means ± standard error of the main of triplicate independent experiments. The IC_{50} values were calculated by using GraphPad 5 software.

observed at the expected regions [25]. The NMR spectra of these compounds showed double signals. This result revealed the presence of rotational isomers existing both *E*- and *Z*-configuration of the compounds due to the N=CH double bond of hydrazide-hydrazone moiety as expected due to the literature survey [26]. The isomeric ratio, calculated using the integral values of the peak pairs was in a range of 1/4–1/6.

The mass spectra of the title compounds were verified by ESI spectra where the *m/z* values of molecular ion peaks were in complete agreement with the calculated molecular weight for each compound. The M^+ ions of title compounds compromised with the calculated molecular weights. The purity levels of compounds were determined by elemental analyses (C, H, N), and the results were within ± 0.4% of the calculated values. The spectral data of all final compounds were reported for the first time with this study.

2.2. Biological activity evaluation and molecular modeling studies

All of the final compounds were evaluated for AChE, BuChE inhibitory activities *in vitro* by the colorimetric method of Ellman et al [27,28], and $Aβ_{42}$ self-aggregation inhibitory potentials were determined by thioflavin-T fluorescence assay [29]. They were also investigated for their antioxidant properties using DPPH [30,31] and ABTS [32,33] radical scavenging assay methods. Their inhibitory activity against AChE, BuChE and Aβ-aggregation were shown in Tables 1 and 2, antioxidant results were shown in Table 3.

The ChE activity results demonstrated that most of the compounds showed inhibitory potential in micromolar range against AChE and/or BuChE enzyme. According to *ee*AChE inhibition results, all compounds exhibited potent AChE inhibitory activity with IC_{50} values ranging between 5.68 and 11.35 μM. For both series **1** and **2**, methyl substitution diminished the AChE inhibition, whereas nitro and nitrile substitutions slightly enhanced the AChE inhibition. When each series was evaluated within themselves, the nitro derivatives **1g** and **2g** were found to be the most potent compounds on AChE with IC_{50} values of 5.68 μM, 6.33 μM, respectively, being nearly two times more potent than rivastigmine (IC_{50} = 10.87 μM) whereas approximately ten times less potent than galantamine (IC_{50} = 0.43 μM). Additionally, these compounds exhibited higher inhibition against AChE than BuChE. Overall, we can suggest that the introduction of a substituent to terminal phenyl ring and the positional change of benzylidene-carbohydrazide moiety on piperidine ring maintained AChE inhibitory activity but not displayed a considerable improvement. Based on the molecular

Table 2
In vitro *hu*AChE, *hu*BuChE inhibitory activities of the final compounds.

Compound	IC_{50} ± SEM (μM)[a]		Selectivity AChE/BuChE
	*hu*AChE	*hu*BuChE	
1a	69.17 ± 5.17	3.23 ± 0.13	21.41
1b	59.06 ± 5.63	39.59 ± 0.86	1.49
1c	49.92 ± 1.31	30.88 ± 0.93	1.62
1d	66.67 ± 3.86	7.62 ± 0.42	8.75
1e	48.82 ± 1.67	4.66 ± 0.20	10.48
1f	35.89 ± 1.81	4.12 ± 0.06	8.71
1g	11.25 ± 0.42	11.86 ± 0.41	0.95
1h	46.78 ± 2.71	49.56 ± 3.03	0.94
1i	23.55 ± 0.45	11.34 ± 0.27	2.08
1j	17.90 ± 0.59	9.10 ± 1.45	1.97
2a	74.40 ± 7.46	4.69 ± 2.93	15.86
2b	42.21 ± 1.845	7.76 ± 0.47	5.44
2c	23.82 ± 1.45	> 100	
2d	49.46 ± 1.29	57.29 ± 1.67	0.86
2e	18.54 ± 0.81	15.35 ± 0.45	1.21
2f	21.37 ± 0.47	11.43 ± 0.57	1.87
2g	8.80 ± 0.10	> 100	
2h	15.73 ± 0.81	> 100	
2i	11.02 ± 0.60	> 100	
2j	9.56 ± 0.33	62.60 ± 1.71	
Tacrine HCl	0.52 ± 0.09	0.11 ± 0.0013	4.73
Galantamine	0.52 ± 0.06	14.92 ± 0.57	0.03
Rivastigmine	9.29 ± 0.33	6.07 ± 0.27	1.53

The IC_{50} values were calculated by using GraphPad 5 software.
[a] Data are means ± standard error of the main of triplicate independent experiments.

Table 3
In vitro DPPH and ABTS radical scavenging capacities of the final compounds.

Compound	DPPH scavenging activity (% Inhibition)		ABTS scavenging activity (% Inhibition)	
	10^{-4} M ± std	10^{-3} M ± std	10^{-4} M ± std	10^{-3} M ± std
1a	12.91 ± 0.001	12.96 ± 0.004	nd	2.81 ± 0.0002
1b	13.60 ± 0.002	12.12 ± 0.006	nd	2.96 ± 0.0001
1c	nd	nd	10.23 ± 0.001	32.30 ± 0.000
1d	nd	nd	nd	nd
1e	nd	nd	nd	nd
1f	nd	nd	nd	nd
1g	15.14 ± 0.010	37.80 ± 0.017	nd	nd
1h	nd	nd	nd	nd
1i	24.39 ± 0.005	46.58 ± 0.002	44.97 ± 0.002	85.62 ± 0.000
1j	30.27 ± 0.012	54.90 ± 0.007	63.73 ± 0.001	85.56 ± 0.000
2a	13.93 ± 0.130	8.15 ± 0.006	0.31 ± 0.005	7.87 ± 0.004
2b	7.60 ± 0.009	7.52 ± 0.009	nd	8.80 ± 0.004
2c	8.23 ± 0.009	8.81 ± 0.004	nd	15.15 ± 0.004
2d	7.28 ± 0.009	8.01 ± 0.009	nd	5.92 ± 0.004
2e	5.85 ± 0.010	8.47 ± 0.005	0.25 ± 0.002	6.23 ± 0.002
2f	8.04 ± 0.012	8.55 ± 0.004	nd	4.28 ± 0.001
2g	6.82 ± 0.006	13.26 ± 0.017	nd	10.18 ± 0.003
2h	6.12 ± 0.007	12.14 ± 0.028	nd	5.25 ± 0.007
2i	15.26 ± 0.011	26.99 ± 0.005	54.79 ± 0.004	86.90 ± 0.000
2j	20.11 ± 0.028	31.82 ± 0.003	60.07 ± 0.006	87.02 ± 0.001
Trolox	93.94 ± 0.001	93.95 ± 0.001	35.85 ± 0.003	92.93 ± 0.001

nd: not determined.

modeling studies of the most active compound inside the active gorge of *Tc*AChE, compound **1g** settled from the deep to the entrance of the gorge (Fig. 1). *p*-Nitrobenzylidene terminal of the molecule oriented near the entrance of the gorge and the benzyl terminal reached towards the hydrophobic pocket involving Trp84. Binding interactions of the molecule in *Tc*AChE were seen as follows: an intramolecular hydrogen bond; a hydrogen bond between the hydrazone nitrogen and the side chain of Tyr121 that is located at the middle of the gorge which is the narrow part of the active site; a hydrogen bond between the piperidine nitrogen and the water molecule in the active site. Since the hydrazide-hydrazone moiety is the core of all the final compounds, the hydrogen bond between Tyr121 and the hydrazide-hydrazone nitrogen may be the motive of the close AChE inhibitory activity results. However, due to the molecular interactions of compound **1g** and the validation studies of donepezil, we can suggest that even though the molecule was headed towards the deep of the gorge, it could not reach up to Trp84 and form a π-π interaction as in donepezil. Likewise, the *p*-nitrobenzylidene terminal was located near the entrance but could not reach to Trp279 and interact like donepezil. Molecular dynamics simulation was also carried out to the selected pose of compound **1g** inside the active gorge of *Tc*AChE in order to test the stability of the binding interactions for 80 ns. The results demonstrated that the ligand was stable but the phenyl part of the compound was slightly moving in the active gorge without losing the key hydrogen bond. So, we can speculate that if the molecule was longer, the binding interactions could have been more with the key residues (Fig. S1).

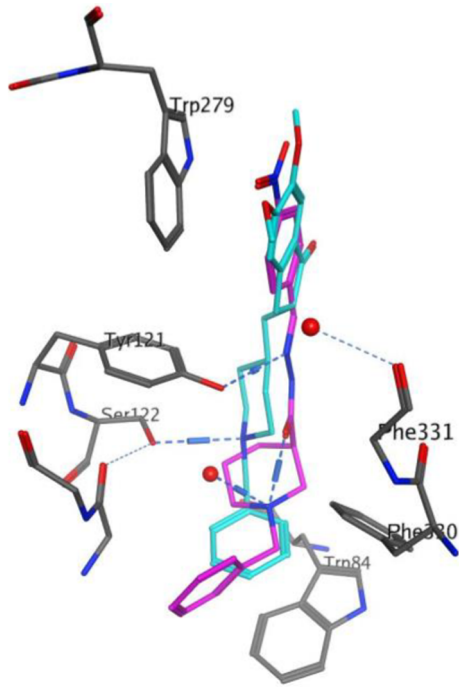

Fig. 1. Binding modes of donepezil and compound **1g** inside *Tc*AChE (pdb code 1EVE). Donepezil is represented as blue sticks; compound **1g** as pink sticks; the most involved residues are named and represented as gray sticks; water molecules are represented as red spheres and the hydrogen bonds are seen as blue dashed lines.

The inhibitory activity of the compounds against *hu*AChE were reported in Table 2. Generally series **2** possessed slightly better activity than series **1**. When each series was evaluated in itself, nitro, dimethyl and diethyl derivatives (**1g**, **1i**, **1j** and **2g**, **2i**, **2j**) exhibited higher inhibition on *hu*AChE enzyme and in each series, the nitro derivatives (**1g** and **2g**) were the most active compounds with an IC_{50} value of 11.25 and 8.80 μM, respectively. The activity results indicated that the introduction of a substituent on phenyl ring enhanced the inhibition potency for *hu*AChE, therefore the presence of a substituent may be considered to have a positive influence on inhibitory activity. Concerning halogen substitutions, the replacement of florine atom with a chlorine and bromine led to an increase on AChE inhibitory activity. In terms of the most active compound (**2g**), molecular modeling studies inside the active gorge of *hu*AChE were performed and the results revealed that compound **2g** settled from the deep to the entrance of the gorge but unlike compound **1g**-*Tc*AChE complex, the protonated piperidine nitrogen and the phenyl group of Tyr341 formed a cation-π interaction (Fig. 2). Molecular dynamics simulation for 80 ns suggested that the molecule was stable in the active gorge but lost its π-π interactions of two terminal phenyl rings in the first 7 ns in order to settle in the active site while conserving the cation-π interaction for the whole simulation (Fig. S2)

Regarding *eq*BuChE inhibitory results, most of the compounds

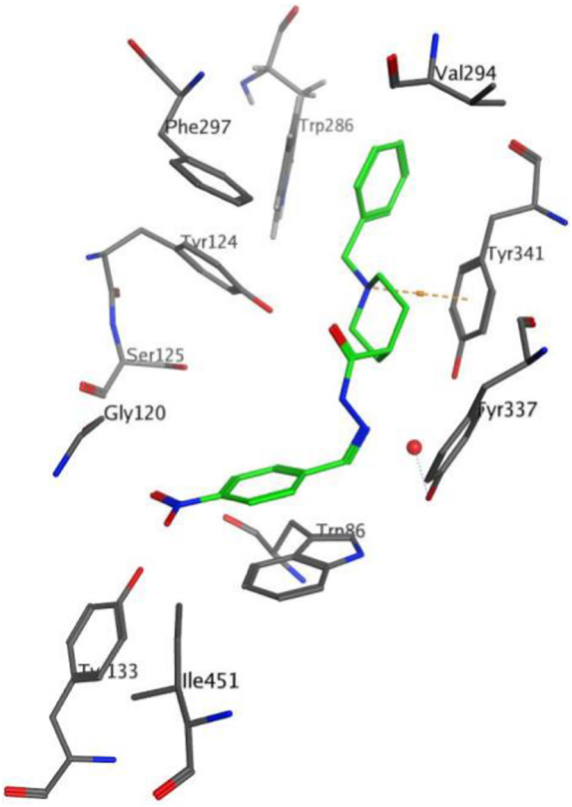

Fig. 2. Binding mode of compound **2g** inside *hu*AChE (pdb code 4EY7). Compound **2g** was represented as green sticks; water molecule as red sphere; the most involved residues are named and represented as gray sticks; hydrogen bonds and cation-π interaction are seen as blue and orange dashed lines, respectively.

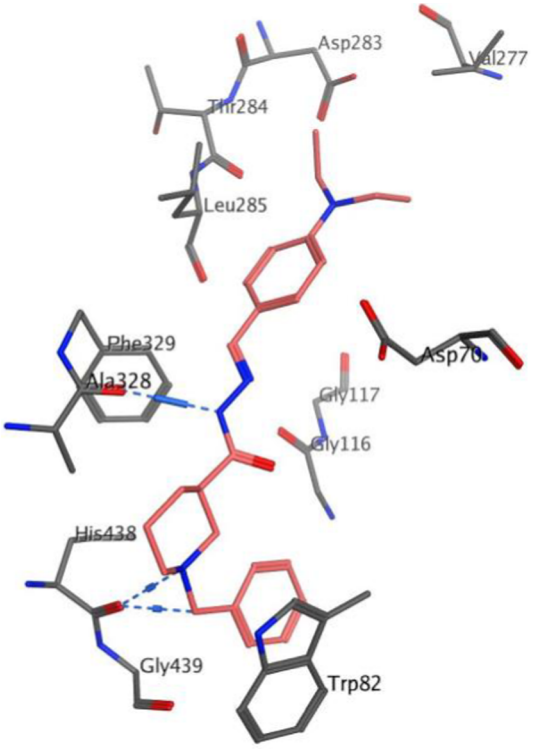

Fig. 3. Binding mode of compound **1j** inside homology model BuChE. Compound **1j** is represented as salmon pink sticks while the involved residues are named and represented as gray sticks. Hydrogen bonds are seen as blue dashed lines.

exhibited BuChE inhibitory activity. Diethylamino derivative **1j** showed the best inhibitory activity with a submicromolar IC_{50} value of 0.81 μM and more potent than rivastigmine (IC_{50} = 5.13 μM), galantamine (IC_{50} = 14.92 μM) and less potent than tacrine (IC_{50} = 0.0098 μM). It was also10-times more active than its congener **2j** (IC_{50} = 8.20 μM) having benzylidene-carbohydrazide moiety at C-4 position instead C-3 on piperidine ring. The positional change of this moiety from C-4 (**2j**) to C-3 (**1j**) on piperidine ring caused a very remarkable improvement in inhibiting BuChE. Dimethylamino derivative **1i** was the second most active with an IC_{50} value of 4.54 μM. On the other hand, in both series (series **1** and **2**) the insertion of nitro, nitrile and methoxy group to phenyl ring remarkably decreased the BuChE inhibitory activity. Molecular modeling studies between the homology model BuChE and compound **1j** possessed noteworthy binding interactions (Fig. 3). NH part of the hydrazide-hydrazone moiety formed a hydrogen bond with Ala328 which replaces Phe330 in AChE located at the middle and narrow part of the gorge [34]. Another hydrogen bond was observed between the protonated piperidine N and His438 which is one of the key residues of the catalytic triad of BuChE [34]. Moreover, molecular dynamics simulation for 80 ns was carried out and the resulting data revealed that the ligand was stable for the whole MD without losing the key interactions. According to the orientation of the ligand in model BuChE, we can suggest that the high activity result may be related to the interaction of the ligand with the key residues (Fig. S3).

*hu*BuChE inhibitory activity of the final compounds were presented in Table 2. Generally, shifting of the hydrazide functional group from C-4 (series **2**) to C-3 (series **1**) position on piperidine ring led to an enhancement in the inhibitory effect on *hu*BuChE. Among series **1**, **1a** and its derivatives bearing florine (**1d**), chlorine(**1e**), bromine (**1f**), nitro (**1g**), dimethylamino (**1i**), diethylamino (**1j**) groups exhibited moderate activity with IC_{50} value in a range of 3.23–11.86 μM. The introduction of a substituent at *para* position of the phenyl ring did not improve the activity, but as for compounds **1e** and **1f** bearing chlorine and bromine, the inhibitory potency was maintained. From the results of the compounds in series **2**, compounds having methyl (**2b**), chlorine (**2e**), bromine (**2f**) substitutions on phenyl ring and their non-substituted analogue (**2a**) displayed moderate *hu*BuChE inhibition with IC_{50} values ranging from 4.69 to 15.35 μM. Overall, the most active compound on *hu*BuChE is compound **1a** with IC_{50} value of 3.23 μM. Molecular interactions of compound **1a** inside *hu*BuChE active gorge were located at the deep of the gorge. The protonated nitrogen atom formed a cation-π interaction with the indole ring of Trp82 (Fig. 4).

Kinetic studies were carried out to investigate the inhibition mechanism and inhibition constant, K_i of the most active compounds **1g** (on *ee*AChE) and **1j** (on *eq*BuChE) based on the Ellman's method as described for AChE/BuChE evaluation. The graphical analysis of steady-state inhibition data for compound **1g** for *ee*AChE and compound **1j** for *eq*BuChE were shown in Figs. 5 and 6, respectively. The obtained Lineweaver-Burk plots [35], double reciprocal plots of Michaelis-Menten parameters, represented both increasing slopes (decreased V_{max}) and intercepts (higher K_m) at increasing concentrations of the inhibitor. This characteristic pattern suggested a mixed-type inhibition between *ee*AChE and **1g**; *eq*BuChE and **1j**, therefore revealed that both compounds might be able to interact with CAS and PAS of the respective enzymes, which were in consistent with the results from molecular modeling study of **1g** and **1j**. The K_i values of **1g** was obtained 1.3 μM for *ee*AChE and 0.24 μM for *eq*BuChE (Table 4).

$A\beta_{42}$ self-aggregation inhibitory activity was performed at 100 μM and 25 μM. Based on the inhibition data, series **1** generally exhibited better inhibitor activity than series **2** and all compounds, except for nitrile derivatives (**1h**, **2h**), showed an inhibition ratio between 79.34 and 15.09% at 100 μM, 53.18–3.66% at 25 μM. Regarding series **1**, introduction of a substituent at *para* position of the benzylidene moiety

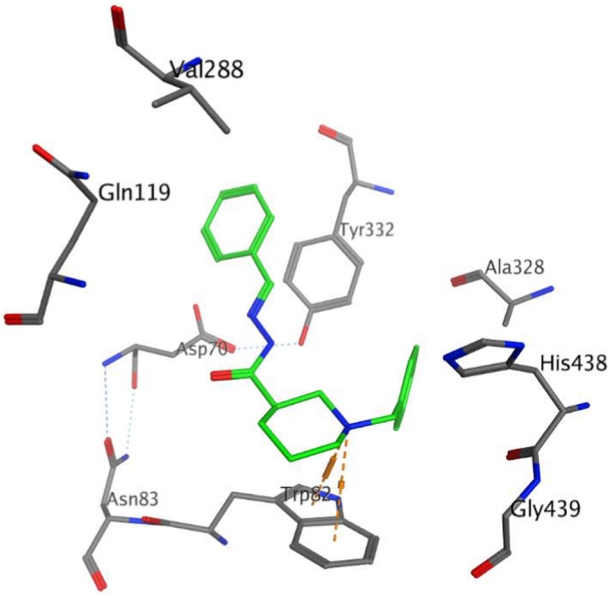

Fig. 4. Binding mode of compound **1a** inside *hu*BuChE (pdb code 2PM8). Compound **1a** is represented as purple sticks while the involved residues are named and represented as gray sticks. Hydrogen bonds and cation-π interaction are seen as blue and orange dashed lines, respectively.

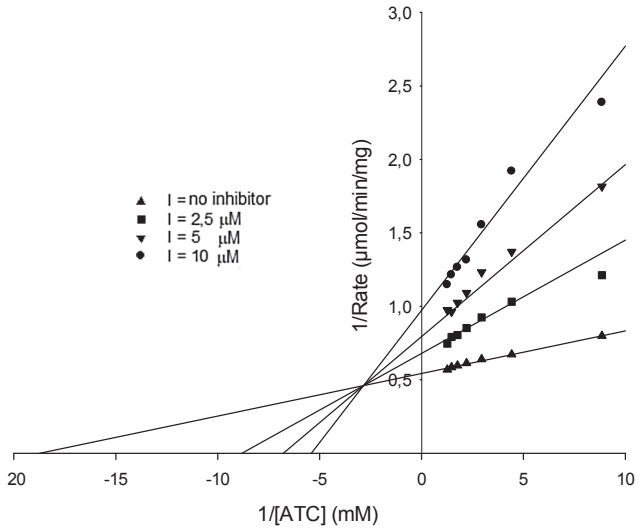

Fig. 5. Lineweavere-Burk plot for the inhibition of *ee*AChE by compound **1g** at different concentrations with acetylthiocholine (ATC) as substrate.

had a positive effect on the inhibitory potency. Except for nitrile (**1h**) and dimethylamino (**1i**) derivatives, series **1** displayed an inhibition over 49% at 100 μM and over 26% at 25 μM concentration. Moreover, methyl (**1b**), bromo (**1f**), nitro (**1g**) and diethylamino (**1j**) derivatives conserved their inhibitory activity even the concentration decreased 1/4 ratio (25 μM). On the other hand, in series **2**, diethylamino derivative (**2j**) with a ratio of 59.98% at 100 μM and 40.30% at 25 μM possessed the best inhibitory activity. To sum up, the nitro derivative (**1g**) which was found to be the most potent against AChE, also exhibited the highest inhibitory activity towards $A\beta_{42}$-aggregation with a ratio of 79.34% at 100 μM and 53.18% at 25 μM.

Antioxidant activities of the title compounds were evaluated using two different assays at concentrations of 1 mM and 100 μM. The scavenger capacity was tested by measuring the decrease the absorption of DPPH [30,31] and ABTS [32,33] radicals. The results revealed that some of the compounds had radical scavenging capacity in a range of

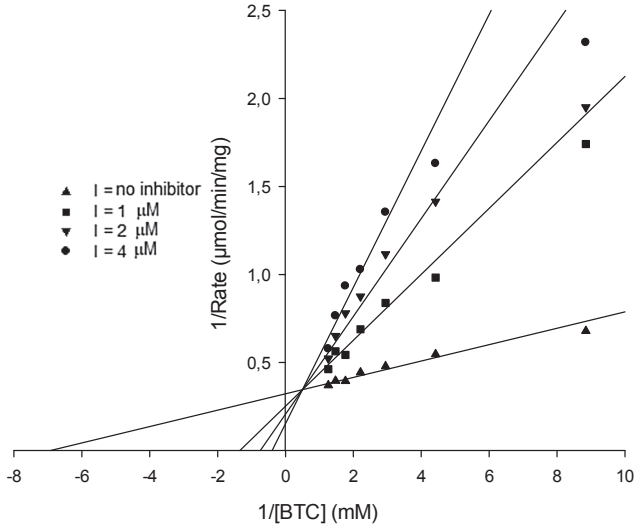

Fig 6. Lineweavere-Burk plot for the inhibition of *eq*BuChE by compound **1j** at different concentrations with butyrylthiocholine (BTC) as substrate.

87.02–85.56% in ABTS; 54.90–26.99% in DPPH at 10^{-3} M and 63.73–44.97% in ABTS; 30.27–15.26% in DPPH at 10^{-4} M. The highest antioxidant activity was obtained with dimethylamino (**1i**, **2i**) and diethylamino (**1j**, **2j**) substituents on benzylidene moiety and IC_{50} values of these compounds were also tested. The results were presented in Table 5. According to activity results, compounds **1i** and **1j** showed better DPPH antioxidant capacity, whereas compounds **2j** and **2i** displayed higher ABTS antioxidant activity. Moreover, **1j, 2j** and **2i** have remarkably higher ABTS radical scavenging potency when compared with the reference compound trolox. In contrast, all compounds had lower DPPH radical scavenging activity than trolox.

To predict the pharmacokinetic profiles of the final compounds, their physicochemical properties (partition coefficient (logP), distribution coefficient at pH 7.4 (logD); molecular weight (MW); topological polar surface area (TPSA); number of hydrogen-bond donors (HBD); and number of hydrogen-bond acceptor (HBA)) were calculated by MOE programme [36] and presented in Table 6. These parameters are the most representative features to determine the ADME profile, as well as the ability of a compound in reaching CNS. Molecular weight MW of the compounds was found between 322 and 401 Da; log P and SlogP were in the range of 3.7070–4.8450 and 1.7699–2.7444; number of H-bond donors and acceptors were 2 and 4–7, respectively. Not only the title compounds met the criteria for Lipinski's "rule of five", their log D (1.4089–3.075) and TPSA (45.90–91.72) values were in acceptable range for potential BBB penetration [37,38]. Therefore, it might be predicted that the compounds have a favorable pharmacokinetic profiles.

3. Conclusion

In this study, two series of compounds bearing piperidinehydrazide-hydrazone core were designed, synthesized and AChE, BuChE and Aβ self-aggregation inhibitory activities, as well as antioxidant capacities were evaluated. Most of the compounds exhibited AChE and BuChE inhibitory activity. In general, the positional change of benzylidene-carbohydrazide fragment from C-4 to C-3 on piperidine affect the ChE activity and Aβ inhibitions. Besides, most of the compounds displayed Aβ anti-aggregation properties. Moreover, compounds having dimethylamino (**1i**, **2i**) and diethylamino substituent (**1j**, **2j**) behaved as strong antioxidant agents. Kinetic studies revealed that compound **1g** and **1j** possessed mixed type inhibition with the ability to bind both PAS and CAS of the respective enzyme and molecular modeling studies supported this arguement.

Table 4
Inhibition constants (K_i) and Michaelis-Menten constants (K_m) for *ee*AChE and *eq*BuChE inhibition by compound **1g** and **1j**.

Compound	Enzyme	Inhibition mechanism	K_i (μM) ± std	K_m (mM) ± std	V_{max}	R^2
1g	*ee*AChE	mixed	1.3 ± 0.128	0.05 ± 0.004	1.84 ± 0.002	0.991
1j	*eq*BuChE	mixed	0.24 ± 0.033	0.14 ± 0.015	3.10 ± 0.086	0.972

The parameters were calculated by using SigmaPlot software.

Table 5
IC_{50} values of the most active compounds for antioxidant activity.

Compound	DPPH scavenging activity IC_{50} ± std (μM)[a]	ABTS scavenging activity IC_{50} ± std (μM)[a]
1i	889 ± 3.13	149 ± 0.06
1j	623 ± 3.96	68 ± 1.58
2i	1180 ± 2.62	63 ± 0.25
2j	1785 ± 3.13	50 ± 0.93
Trolox	28 ± 0.32	118 ± 0.93

The IC_{50} values were calculated by using GraphPad 5 software.
[a] Data are means ± standard error of the main of triplicate independent experiments.

Table 6
Physicochemical properties of the final compounds.

Compound	MW	logP	SlogP	logD (pH 7.4)	TPSA	HBD	HBA
1a	322.4320	4.0470	1.8982	2.4085	45.90	2	4
1b	336.4590	4.3450	2.2066	2.9039	45.90	2	4
1c	352.4580	4.0030	1.9068	2.3008	55.13	2	5
1d	340.4220	4.2000	2.0373	2.4548	45.90	2	4
1e	356.8770	4.6390	2.5516	3.0745	45.90	2	4
1f	401.3280	4.8450	2.6607	1.4089	45.90	2	4
1g	367.4290	3.9820	1.8064	2.3936	91.72	2	7
1h	347.4420	3.7070	1.7699	2.4994	69.69	2	5
1i	365.5010	3.9620	1.9642	2.4969	49.14	2	4
1j	393.5550	4.6400	2.7444	3.0020	49.14	2	5
2a	322.4320	4.0470	1.8982	1.7455	45.90	2	4
2b	336.4590	4.3450	2.2066	2.2409	45.90	2	4
2c	352.4580	4.0030	1.9068	1.6375	55.13	2	5
2d	340.4220	4.2000	2.0373	1.7922	45.90	2	4
2e	356.8770	4.6390	2.5516	2.4196	45.90	2	4
2f	401.3280	4.8450	2.6607	2.5596	45.90	2	4
2g	367.4290	3.9820	1.8064	1.7265	91.72	2	7
2h	347.4420	3.7070	1.7699	1.8342	69.69	2	5
2i	365.5010	3.9620	1.9642	1.8380	49.14	2	4
2j	393.5550	4.6400	2.7444	2.3432	49.14	2	5

The values were calculated by using MOE.

In conclusion, ChE, Aβ inhibition and antioxidant studies suggests that compound **1g** and **1j** exhibited the best profile to be considered as multi-target lead compounds for the treatment of AD.

4. Materials and methods

4.1. Chemistry

Melting points were determined using a Stuart SMP30 (Staffordshire, ST15 OSA, U.K.) melting point apparatus and are not corrected. The IR spectra of the compounds were monitored by attenuated total reflectance (ATR) (PerkinElmer Spectrum 100 FT-IR, Shelton, USA). ^{1}H- and ^{13}C NMR spectra were recorded with a Varian AS 400 Mercury Plus NMR spectrometer (Varian, Palo Alto, CA, U.S.A.) operated at 400 and 100 MHz for ^{1}H and ^{13}C, respectively, in deuterochloroform ($CDCl_3$). Chemical shifts are given in ppm (δ) with tetramethylsilane (TMS) as an internal standard. Abbreviations for data quoted are: s (singlet), d (doublet), t (triplet), q (quartet), quin (quintet), sept (septet), td (triplet-doublet), m (multiplet), bs (broad singlet). Mass spectra (ESI-MS) were measured on a Thermo MSQ Plus LC/MS (Thermoscientific Inc., San Jose, CA). Elemental analyses (C, H, N) were performed by Leco TruSpec Micro (Leco, St. Joseph, MI). The analytical results for the elements were within ± 0.4% of the theoretical values. All chemicals, reagents and solvents used for synthesis were high-grade commercial products and they were purchased from Sigma-Aldrich, Fluka and Merck Companies. Reactions were checked by TLC on pre-coated silica gel aluminum plates (Kieselgel 60, F254, E. Merck, Germany); spots were visualized by UV at 254 nm.

4.1.1. General procedure for synthesis of ethyl 1-benzylpiperidine-3-carboxylate/ethyl 1-benzylpiperidine-4-carboxylate

Ethyl nipecotate/Ethyl isonipecotate (0.014 mol/0.03 mol) and triethylamine (0.014 mol/0.06 mol) were dissolved in 30 mL acetonitrile and stirred for 5–10 min in an ice bath under argon gas. Benzyl chloride (0.007 mol/0.02 mol) was added in one portion to this mixture and then the resulting mixture was stirred at room temperature for 8–48 h under argon gas. The precipitate was removed, acetonitrile was evaporated under reduced pressure and the organic layer was extracted with diethyl ether. The combined organic extracts were dried over anhydrous sodium sulfate and concentrated in vacuo. The crude product was purified by column chromatography (ethyl acetate/*n*-hexane) to give ethyl 1-benzylpiperidine-3-carboxylate as a yellowish oil. Ethyl 1-benzylpiperidine-4-carboxylate was obtained as a pure yellowish oil after vacuo without further purification.

4.1.2. General procedure for synthesis of N-substitutednipecotic acid hydrazids/N-substitutedisonipecotic acid hydrazids

Each ethyl *N*-substituted nipecotate derivative/ethyl *N*-substituted isonipecotate derivative (1 mol) in 30 mL ethanol and hydrazinium hydroxide (10 mol) were heated under microwave irradiation (130 °C, 300 W) or refluxed for 24–48 h in an oil bath. After completion of the reaction (TLC), ethanol was evaporated and the residue was extracted with dichloromethane or diethyl ether. The solvent was evaporated under reduced pressure until an oily residue occured. Then *n*-hexane was added to the residue to give the title compound as a white solid. The precipitated crystals were separated by filtration.

4.1.3. General procedure for synthesis of the final compounds (1a–2j)

Obtained hydrazide derivative in the previous step (1 mol) in 25–30 mL ethanol was condensated with 2 mol appropriate benzaldehydes (benzaldehyde, 4-methylbenzaldehyde, 4-methoxybenzaldehyde, 4-fluorobenzaldehyde, 4-chlorobenzaldehyde, 4-bromobenzaldehyde, 4-nitrobenzaldehyde, 4-cyanobenzaldehyde, 4-dimethylaminobenzaldehyde, 4-diethylaminobenzaldehyde) under reflux for 4–18 h. The mixture was evaporated to dryness and the crude product was dissolved in ethanol and deionized water was added dropwise to yield the pure final compounds or purified by column chromatography [chloroform:methanol (10:1) or *n*-hexane:ethylacetate:methanol (5:3:1,5)].

4.1.3.1. 1-benzyl-N′-benzylidenepiperidine-3-carbohydrazide (1a). Yield 55%; mp 138 °C. IR ν_{max}(cm^{-1}) 3178, 3086, 2958, 2933, 2788, 1659, 1611, 1494, 1449, 1398, 1368, 1254, 1211, 1105, 746, 687. ^{1}H NMR (400 MHz, $CDCl_3$) δ 1.61–1.78 (3H, m, piperidine-H), 1.99–2.23 (2H, m, piperidine-H), 2.31–2.36 (1H, m, piperidine-H), 2.67–2.69 (1H, m, piperidine-H), 3.01 (1H, d, J = 10.9 Hz, piperidine-H), 3.11 (1H, d, J = 11.8 Hz, piperidine-H), 3.47–3.61 (2H, m, N−CH_2), 7.30–7.41 (8H,

m, H-2′, H-3′, H-4′, H-5′, H-6′, H-3″, H-4″, H-5″), 7.71–7.76 (2H, m, H-2″, H-6″), 8.02 (1H, s, N=CH), 11.47 (1H, bs, NH) ppm. ^{13}C NMR (100 MHz, $CDCl_3$) δ 22.55, 26.90, 41.19, 53.96, 54.04, 63.39, 127.14, 127.58, 128.13, 128.58, 129.37, 130.24, 133.92, 137.38, 147.64, 171.62 ppm. ESI-MS *m/z* (%): 322 (M + H, 100). Anal. calcd. for $C_{20}H_{23}N_3O$: C, 74.74; H, 7.21; N, 13.07. Found: C, 75.07; H, 7.32; N, 12.79.

4.1.3.2. 1-benzyl-N′-(4-methylbenzylidene)piperidine-3-carbohydrazide ***(1b)***. Yield 36%; mp 179 °C. IR ν_{max}(cm^{-1}) 3178, 3084, 3028, 2955, 2853, 2793, 2753, 1655, 1613, 1492, 1449, 1401, 1368, 1255, 1211, 1103, 811, 741. ^{1}H NMR (400 MHz, $CDCl_3$) δ 1.60–1.78 (3H, m, piperidine-H), 2.09–2.23 (2H, m, piperidine-H), 2.32 (1H, d, J = 11.0 Hz, piperidine-H), 2.38 (3H, s, CH_3), 2.67 (1H, bs, piperidine-H), 3.01 (1H, d, J = 11.6 Hz, piperidine-H), 3.11 (1H, d, J = 11.3 Hz, piperidine-H), 3.48–3.60 (2H, m, N−CH_2), 7.20 (2H, d, J = 8.2, Hz, H-3″, H-5″), 7.30–7.40 (5H, m, H-2′, H-3′, H-4′, H-5′, H-6′), 7.63 (2H, d, J = 8.1 Hz, H-2″, H-6″), 7.98 (1H, s, N=CH), 11.41 (1H, bs, NH) ppm. ^{13}C NMR (100 MHz, $CDCl_3$) δ 21.48, 22.33, 26.86, 41.04, 54.06, 54.24, 63.43, 127.56, 127.76, 128.60, 129.33, 129.36, 131.18, 137.29, 140.59, 147.67, 171.44 ppm. ESI-MS *m/z* (%): 336 (M + H, 100). Anal. calcd. for $C_{21}H_{25}N_3O$: C, 75.19; H, 7.51; N, 12.53. Found: C, 75.44; H, 7.40; N, 12.14.

4.1.3.3. 1-benzyl-N′-(4-methoxybenzylidene)piperidine-3-carbohydrazide ***(1c)***. Yield 47%; mp 148 °C. IR ν_{max}(cm^{-1}) 3175, 3081, 3025, 2958, 2935, 2843, 2795, 2754, 1656, 1609, 1574, 1516, 1494, 1450, 1421, 1400, 1368, 1248, 1210, 1169, 1035, 830, 743, 701. ^{1}H NMR (400 MHz, $CDCl_3$) δ 1.59–1.78 (3H, m, piperidine-H), 2.08–2.23 (2H, m, piperidine-H), 2.33 (1H, d, J = 11.1 Hz, piperidine-H), 2.67 (1H, bs, piperidine-H), 2.99 (1H, d, J = 11.7 Hz, piperidine-H), 3.10 (1H, d, J = 12.0 Hz, piperidine-H), 3.48–3.61 (2H, m, N−CH_2), 3.84 (3H, s, OCH_3), 6.91 (2H, d, J = 8.6, Hz, H-3″, H-5″), 7.32–7.40 (5H, m, H-2′, H-3′, H-4′, H-5′, H-6′), 7.68 (2H, d, J = 8.8 Hz, H-2″, H-6″), 7.95 (1H, s, N=CH), 11.36 (1H, bs, NH) ppm. ^{13}C NMR (100 MHz, $CDCl_3$) δ 22.43, 26.86, 41.07, 53.99, 54.35, 55.32, 63.39, 114.08, 126.57, 127.73, 128.57, 129.15, 129.37, 137.28, 147.42, 161.38, 171.32 ppm. ESI-MS *m/z* (%): 352 (M + H, 100). Anal. calcd. for $C_{21}H_{25}N_3O_2$: C, 71.77; H, 7.17; N, 11.96. Found: C, 71.74; H, 7.08; N, 12.02.

4.1.3.4. 1-benzyl-N′-(4-fluorobenzylidene)piperidine-3-carbohydrazide ***(1d)***. Yield 66%; mp 147 °C. IR ν_{max}(cm^{-1}) 3182, 3083, 2956, 2860, 2787, 2744, 1662, 1615, 1603, 1504, 1493, 1449, 1400, 1367, 1255, 1232, 1210, 1107, 744, 700. ^{1}H NMR (400 MHz, $CDCl_3$) δ 1.59–1.77 (3H, m, piperidine-H), 2.08–2.11 (1H, m, piperidine-H), 2.19 (1H, t, J = 12.0 Hz, piperidine-H), 2.31–2.34 (1H, m, piperidine-H), 2.67 (1H, bs, piperidine-H), 2.92 (1H, d, J = 10.7 Hz, piperidine-H), 3.10 (1H, d, J = 11.1 Hz, piperidine-H), 3.47–3.60 (2H, m, N−CH_2), 7.05–7.11 (2H, m, H-3″, H-5″), 7.32–7.40 (5H, m, H-2′, H-3′, H-4′, H-5′, H-6′), 7.69–7.74 (2H, m, H-2″, H-6″), 8.00 (1H, s, N=CH), 11.48 (1H, bs, NH) ppm. ^{13}C NMR (100 MHz, $CDCl_3$) δ 22.44, 26.86, 41.11, 54.00, 54.25, 63.38, 115.64, 115.86, 127.74, 128.58, 129.33, 129.35, 129.41, 130.16, 130.19, 137.32, 146.36, 162.70, 165.19, 171.64 ppm. ESI-MS *m/z* (%): 340 (M + H, 100). Anal. calcd. for $C_{20}H_{22}FN_3O$: C, 70.77; H, 6.53; N, 12.38. Found: C, 70.96; H, 6.67; N, 12.17.

4.1.3.5. 1-benzyl-N′-(4-chlorobenzylidene)piperidine-3-carbohydrazide ***(1e)***. Yield 36%; mp 174 °C. IR ν_{max}(cm^{-1}) 3178, 3080, 3056, 2941, 2857, 2790, 2751, 1663, 1610, 1490, 1449, 1399, 1368, 1255, 1210, 1139, 1104, 1089, 1070, 824, 743, 724, 699. ^{1}H NMR (400 MHz, $CDCl_3$) δ 1.66–1.77 (3H, m, piperidine-H), 2.10 (1H, d, J = 12.1 Hz, piperidine-H), 2.19 (1H, t, J = 10.8 Hz, piperidine-H), 2.31–2.34 (1H, m, piperidine-H), 2.68 (1H, bs, piperidine-H), 3.00–3.03 (1H, m, piperidine-H), 3.11 (1H, d, J = 12.2 Hz, piperidine-H), 3.46–3.61 (2H, m, N−CH_2), 7.30–7.38 (7H, m, H-2′, H-3′, H-4′, H-5′, H-6′, H-3″, H-5″), 7.66 (2H, d, J = 8.5 Hz, H-2″, H-6″), 7.99 (1H, s, N=CH), 11.54 (1H, bs, NH) ppm. ^{13}C NMR (100 MHz, $CDCl_3$) δ 22.38, 26.84, 41.07, 54.04, 54.16, 63.38, 127.78, 128.60, 128.65, 128.89, 129.35, 132.48, 136.10, 137.26, 146.20, 171.68 ppm. ESI-MS *m/z* (%): 356 (M + H, 100), 358 (M + H + 2, 42). Anal. calcd. for $C_{20}H_{22}ClN_3O$: C, 67.50; H, 6.23; N, 11.81. Found: C, 67.69; H, 6.28; N, 12.18.

4.1.3.6. 1-benzyl-N′-(4-bromobenzylidene)piperidine-3-carbohydrazide ***(1f)***. Yield 44%; mp 180 °C. IR ν_{max}(cm^{-1}) 3178, 3093, 3056, 2944, 2930, 2790, 2753, 1665, 1610, 1487, 1449, 1397, 1368, 1255, 1211, 1138, 936, 837, 742, 700. ^{1}H NMR (400 MHz, $CDCl_3$) δ 1.51–1.77 (3H, m, piperidine-H), 2.10 (1H, d, J = 12.0 Hz, piperidine-H), 2.18 (1H, t, J = 12.0 Hz, piperidine-H), 2.33 (1H, d, J = 11.4 Hz, piperidine-H), 2.68 (1H, bs, piperidine-H), 3.02 (1H, d, J = 11.5 Hz, piperidine-H), 3.11 (1H, d, J = 11.7 Hz, piperidine-H), 3.43–3.61 (2H, m, N−CH_2), 7.25–7.40 (5H, m, H-2′, H-3′, H-4′, H-5′, H-6′), 7.52 (2H, d, J = 8.8 Hz, H-2″, H-6″), 7.60 (2H, d, J = 8.5 Hz, H-3″, H-5″), 7.98 (1H, s, N=CH), 11.54 (1H, bs, NH) ppm. ^{13}C NMR (100 MHz, $CDCl_3$) δ 22.41, 26.84, 41.09, 54.01, 54.17, 63.37, 124.48, 127.78, 128.60, 128.88, 129.36, 131.84, 132.91, 137.26, 146.28, 171.72 ppm. ESI-MS *m/z* (%): 400 (M + H, 100), 402 (M + H + 2, 91). Anal. calcd. for $C_{20}H_{22}BrN_3O$: C, 60.01; H, 5.54; N, 10.50. Found: C, 60.10; H, 5.75; N, 10.45.

4.1.3.7. 1-benzyl-N′-(4-nitrobenzylidene)piperidine-3-carbohydrazide ***(1g)***. Yield 43%; mp 198 °C. IR ν_{max}(cm^{-1}) 3182, 3083, 2958, 2933, 2792, 2752, 1665, 1614, 1600, 1582, 1519, 1491, 1449, 1397, 1338, 1256, 1211, 1150, 1106, 744, 700, 689. ^{1}H NMR (400 MHz, $CDCl_3$) δ 1.73–1.77 (3H, m, piperidine-H), 2.09–2.24 (2H, m, piperidine-H), 2.32–2.36 (1H, m, piperidine-H), 2.70 (1H, bs, piperidine-H), 3.05–3.14 (2H, m, piperidine-H), 3.47–3.63 (2H, m, N−CH_2), 7.19–7.41 (5H, m, H-2′, H-3′, H-4′, H-5′, H-6′), 7.88 (2H, d, J = 8.8 Hz, H-2″, H-6″), 8.16 (1H, s, N=CH), 8.24 (2H, d, J = 8.8 Hz, H-3″, H-5″), 11.80 (1H, bs, NH) ppm. ^{13}C NMR (100 MHz, $CDCl_3$) δ 22.30, 26.82, 41.08, 53.96, 54.04, 63.33, 123.92, 127.89, 127.94, 128.66, 129.38, 137.12, 140.18, 144.69, 148.52, 172.12 ppm. ESI-MS *m/z* (%) 367 (M + H, 100). Anal. calcd. for $C_{20}H_{22}N_4O_3$: C, 65.56; H, 6.05; N, 15.29. Found: C, 65.40; H, 6.23; N, 14.99.

4.1.3.8. 1-benzyl-N′-(4-cyanobenzylidene)piperidine-3-carbohydrazide ***(1h)***. Yield 25%; mp 150 °C. IR ν_{max}(cm^{-1}) 3189, 3082, 3056, 2949, 2864, 2794, 2755, 2227, 1663, 1593, 1554, 1491, 1450, 1400, 1369, 1333, 1210, 1151, 1105, 837, 737, 698. ^{1}H NMR (400 MHz, $CDCl_3$) δ 1.59–1.77 (3H, m, piperidine-H), 2.02–2.26 (2H, m, piperidine-H), 2.36 (1H, d, J = 10.5 Hz, piperidine-H), 2.68 (1H, bs, piperidine-H), 2.91–3.06 (2H, m, piperidine-H), 3.46–3.61 (2H, m, N−CH_2), 7.31–7.38 (5H, m, H-2′, H-3′, H-4′, H-5′, H-6′), 7.65 (2H, d, J = 8.1 Hz, H-2″, H-6″), 7.78 (2H, d, J = 8.1 Hz, H-3″, H-5″), 8.06 (1H, s, N=CH), 11.72 (1H, bs, NH) ppm. ^{13}C NMR (100 MHz, $CDCl_3$) δ 22.42, 26.85, 41.14, 53.99, 54.02, 63.31, 113.20, 118.48, 127.39, 127.74, 128.62, 129.36, 132.35, 137.23, 138.37, 145.14, 172.06 ppm. ESI-MS *m/z* (%): 347 (M + H, 100). Anal. calcd. for $C_{21}H_{22}N_4O$: C, 72.81; H, 6.40; N, 16.17. Found: C, 72.72; H, 6.50; N, 16.23.

4.1.3.9. 1-benzyl-N′-(4-(dimethylamino)benzylidene)piperidine-3-carbohydrazide ***(1i)***. Yield 25%; mp 178 °C. IR ν_{max}(cm^{-1}) 3175, 3033, 2927, 2799, 2755, 1665, 1643, 1611, 1598, 1524, 1452, 1362, 1230, 1197, 1176, 815, 737, 699. ^{1}H NMR (400 MHz, $CDCl_3$) δ 1.54–1.76 (3H, m, piperidine-H), 1.99–2.07 (1H, m, piperidine-H), 2.17–2.24 (1H, m, piperidine-H), 2.36 (1H, d, J = 12.0 Hz, piperidine-H), 2.64 (1H, bs, piperidine-H), 2.89–2.92 (1H, m, piperidine-H), 2.99–3.04 (7H, m, N-$(CH_3)_2$, piperidin-H), 3.45–3.60 (2H, m, N−CH_2), 6.67 (2H, d, J = 8.2 Hz, H-3″, H-5″), 7.25–7.38 (5H, m, H-2′, H-3′, H-4′, H-5′, H-6′), 7.61 (2H, d, J = 8.2 Hz, H-2″, H-6″), 7.89 (1H, s, N=CH), 11.16 (1H, bs, NH) ppm. ^{13}C NMR (100 MHz, $CDCl_3$) δ 22.52, 26.90, 40.13, 41.13, 53.96, 54.52, 63.42, 111.63, 121.53, 127.63, 128.54, 129.10, 129.37, 137.44, 148.40, 151.76, 171.00 ppm. ESI-MS *m/z* (%): 365 (M + H, 100). Anal. calcd. for $C_{22}H_{28}N_4O$: C, 72.50; H, 7.74; N, 15.37. Found: C, 72.39; H, 7.71; N, 15.37.

*4.1.3.10. 1-benzyl-N′-(4-(diethylamino)benzylidene)piperidine-3-carbohydrazide (**1j**).* Yield 21%; mp 174 °C. IR ν_{max}(cm^{-1}) 3183, 3035, 2973, 2933, 2795, 1663, 1644, 1609, 1595, 1566, 1529, 1496, 1453, 1431, 1403, 1353, 1270, 1246, 1196, 1177, 1156, 816, 735, 698. ^{1}H NMR (400 MHz, $CDCl_3$) δ 1.17 (6H, t, J = 7.0 Hz, N−(CH_2−$\underline{CH_3}$)$_2$), 1.54–1.73 (3H, m, piperidine-H), 1.99–2.24 (2H, m, piperidine-H), 2.35 (1H, d, J = 11.3 Hz, piperidine-H), 2.62–2.66 (1H, m, piperidine-H), 2.90 (1H, d, J = 12.0 Hz, piperidine-H), 3.04 (1H, d, J = 10.9 Hz, piperidine-H), 3.38 (4H, q, J = 7.0 Hz, N−($\underline{CH_2}$−CH_3)$_2$), 3.46–3.59 (2H, m, N−CH_2), 6.63 (2H, d, J = 8.9 Hz, H-3″, H-5″), 7.26–7.38 (5H, m, H-2′, H-3′, H-4′, H-5′, H-6′), 7.58 (2H, d, J = 8.7 Hz, H-2″, H-6″), 7.87 (1H, s, N=CH), 11.16 (1H, bs, NH) ppm. ^{13}C NMR (100 MHz, $CDCl_3$) δ 12.60, 22.49, 26.89, 41.12, 44.36, 53.97, 54.52, 63.44, 111.01, 120.62, 127.63, 128.53, 129.36, 129.40, 137.45, 148.49, 149.35, 170.90 ppm. ESI-MS *m/z* (%): 393 (M + H, 100). Anal. calcd. for $C_{24}H_{32}N_4O$: C, 73.43; H, 8.22; N, 14.27. Found: C, 73.46; H, 8.08; N, 13.94.

*4.1.3.11. 1-benzyl-N′-benzylidenepiperidine-4-carbohydrazide (**2a**).* Yield 77%; mp 180 °C. IR ν_{max}(cm^{-1}) 3178, 3065, 2942, 2794, 2754, 1664, 1610, 1600, 1440, 1402, 1340, 1233, 1144, 1116, 757, 736, 690. ^{1}H NMR (400 MHz, $CDCl_3$) δ 1.86–1.97 (4H, m, piperidine-H), 2.13 (2H, td, J = 4.2/10.6 Hz, piperidine-H), 2.99 (2H, d, J = 11.6 Hz, piperidine-H), 3.21 (1H, sept, J = 5.8 Hz, piperidine-H), 3.55 (2H, s, N−CH_2), 7.23–7.44 (8H, m, H-2′, H-3′, H-4′, H-5′, H-6′, H-3″, H-4″, H-5″), 7.63–7.66 (2H, m, H-2″, H-6″), 7.78 (1H, s, N=CH), 9.60 (1H, s, NH) ppm. ^{13}C NMR (100 MHz, $CDCl_3$) δ 28.04, 38.65, 53.21, 63.34, 126.91, 127.06, 128.16, 128.73, 129.08, 129.98, 133.99, 138.57, 143.51, 178.18 ppm. ESI-MS *m/z* (%) 322 (M + H, 100). Anal. calcd. for $C_{20}H_{23}N_3O$: C, 74.74; H, 7.21; N, 13.07. Found: C, 74.52; H, 7.45; N, 12.76.

*4.1.3.12. 1-benzyl-N′-(4-methylbenzylidene)piperidine-4-carbohydrazide (**2b**).* Yield 78%; mp 155 °C. IR ν_{max}(cm^{-1}) 3175, 3073, 3032, 2939, 2797, 2755, 1661, 1607, 1507, 1420, 1406, 1303, 1244, 1167, 744, 699. ^{1}H NMR (400 MHz, $CDCl_3$) δ 1.88–1.94 (4H, m, piperidine-H), 2.13 (2H, td, J = 4.0/10.7 Hz, piperidine-H), 2.39 (3H, s, CH_3), 2.99 (2H, d, J = 12.0 Hz, piperidine-H), 3.23 (1H, sept, J = 5.5 Hz, piperidine-H), 3.50 (2H, s, N−CH_2), 7.21 (2H, J = 8.0 Hz, H-3″, H-5″), 7.31–7.37 (5H, m, H-2′, H-3′, H-4′, H-5′, H-6′), 7.55 (2H, d, J = 8.0 Hz, H-2″, H-6″), 7.79 (1H, s, N=CH), 10.04 (1H, bs, NH) ppm. ^{13}C NMR (100 MHz, $CDCl_3$) δ 21.48, 28.04, 38.61, 53.24, 63.35, 126.90, 127.03, 128.15, 129.07, 129.45, 131.33, 138.62, 140.22, 143.70, 178.15 ppm. ESI-MS *m/z* (%): 336 (M + H, 100). Anal. calcd. for $C_{21}H_{25}N_3O$: C, 75.19; H, 7.51; N, 12.53. Found: C, 74.88; H, 7.45; N, 12.92.

*4.1.3.13. 1-benzyl-N′-(4-methoxybenzylidene)piperidine-4-carbohydrazide (**2c**).* Yield 80%; mp 144 °C. IR ν_{max}(cm^{-1}) 3175, 3081, 3025, 2958, 2935, 2843, 2795, 2754, 1656, 1609, 1574, 1516, 1494, 1450, 1421, 1400, 1368, 1248, 1210, 1169, 1035, 830, 743, 701. ^{1}H NMR (400 MHz, $CDCl_3$) δ 1.86–1.95 (4H, m, piperidine-H), 2.08–2.15 (2H, m, piperidine-H), 2.98 (2H, d, J = 12.0 Hz, piperidine-H), 3.15–3.22 (1H, m, piperidine-H), 3.54 (2H, s, N−CH_2), 3.85 (3H, s, OCH_3), 6.93 (2H, d, J = 8.3 Hz, H-3″, H-5″), 7.23–7.36 (5H, m, H-2′, H-3′, H-4′, H-5′, H-6′), 7.58 (2H, d, J = 8.3 Hz, H-2″, H-6″), 7.70 (1H, s, N=CH), 9.31 (1H, bs, NH) ppm. ^{13}C NMR (100 MHz, $CDCl_3$) δ 28.01, 38.70, 53.23, 55.36, 63.33, 114.24, 126.88, 128.14, 128.54, 129.05, 138.60, 142.93, 147.72, 161.16, 177.57 ppm. ESI-MS *m/z* (%): 352 (M + H, 100). Anal. calcd. for $C_{21}H_{25}N_3O_2$: C, 71.77; H, 7.17; N, 11.96. Found: C, 71.65; H, 7.01; N, 12.15.

*4.1.3.14. 1-benzyl-N′-(4-fluorobenzylidene)piperidine-4-carbohydrazide (**2d**).* Yield 81%; mp 191 °C. IR ν_{max}(cm^{-1}) 3182, 3075, 2946, 2805, 2763, 1665, 1615, 1603, 1504, 1401, 1339, 1271, 1229, 1142, 793, 736, 696. ^{1}H NMR (400 MHz, $CDCl_3$) δ 1.85–1.99 (4H, m, piperidine-H), 2.13 (2H, td, J = 3.5/11.1 Hz, piperidine-H), 2.99 (2H, d, J = 11.6 Hz, piperidine-H), 3.21 (1H, sept, J = 5.3 Hz, piperidine-H), 3.55 (2H, s, N−CH_2), 7.08–7.13 (2H, m, H-3″, H-5″), 7.24–7.37 (5H, m, H-2′, H-3′, H-4′, H-5′, H-6′), 7.62–7.66 (2H, m, H-2″, H-6″), 7.83 (1H, s, N=CH), 10.37 (1H, s, NH) ppm. ^{13}C NMR (100 MHz, $CDCl_3$) δ 28.06, 38.56, 53.20, 63.35, 115.77, 115.99, 126.93, 128.16, 128.81, 128.90, 129.08, 130.28, 130.31, 138.53, 142.55, 162.51, 165.00, 178.42 ppm. ESI-MS *m/z* (%): 340 (M + H, 100). Anal. calcd. for $C_{20}H_{22}FN_3O$. 0.3 C_2H_5OH: C, 70.05; H, 6.79; N, 11.90. Found: C, 70.14; H, 6.75; N, 11.77.

*4.1.3.15. 1-benzyl-N′-(4-chlorobenzylidene)piperidine-4-carbohydrazide (**2e**).* Yield 70%; mp 198 °C. IR ν_{max}(cm^{-1}) 3182, 3067, 3025, 2950, 2799, 2756, 1668, 1612, 1489, 1408, 1402, 1339, 1271, 1144, 1087, 1012, 820, 731, 695. ^{1}H NMR (400 MHz, $CDCl_3$) δ 1.84–1.96 (4H, m, piperidine-H), 2.12 (2H, td, J = 4.2/10.9 Hz, piperidine-H), 2.99 (2H, d, J = 11.3 Hz, piperidine-H), 3.19 (1H, sept, J = 5.8 Hz, piperidine-H), 3.55 (2H, s, N−CH_2), 7.24–7.39 (7H, m, H-2′, H-3′, H-4′, H-5′, H-6′, H-3″, H-5″), 7.58 (2H, d, J = 8.4 Hz, H-2″, H-6″), 7.78 (1H, s, N=CH), 10.10 (1H, s, NH) ppm. ^{13}C NMR (100 MHz, $CDCl_3$) δ 28.04, 38.60, 53.17, 63.33, 126.93, 128.16, 128.18, 129.02, 129.07, 132.50, 135.83, 138.50, 142.25, 178.26 ppm. ESI-MS *m/z* (%): 356 (M + H, 100), 358 (M + H + 2, 37). Anal. calcd. for $C_{20}H_{22}ClN_3O$: C, 67.50; H, 6.23; N, 11.81. Found: C, 67.83; H, 6.34; N, 11.49.

*4.1.3.16. 1-benzyl-N′-(4-bromobenzylidene)piperidine-4-carbohydrazide (**2f**).* Yield 69%; mp 181 °C. IR ν_{max}(cm^{-1}) 3185, 3084, 2949, 2867, 2797, 2753, 1670, 1611, 1486, 1446, 1405, 1398, 1271, 1144, 1008, 928, 735, 695. ^{1}H NMR (400 MHz, $CDCl_3$) δ 1.84–1.96 (4H, m, piperidine-H), 2.12 (2H, td, J = 3.4/11.1 Hz, piperidine-H), 3.00 (2H, d, J = 12.0 Hz, piperidine-H), 3.20 (1H, sept, J = 5.7 Hz, piperidine-H), 3.55 (2H, s, N−CH_2), 7.30–7.38 (5H, m, H-2′, H-3′, H-4′, H-5′, H-6′), 7.50–7.55 (4H, m, H-2″, H-3″, H-5″, H-6″), 7.80 (1H, s, N=CH), 10.40 (1H, bs, NH) ppm. ^{13}C NMR (100 MHz, $CDCl_3$) δ 28.05, 38.55, 53.17, 63.34, 124.13, 126.95, 128.17, 128.42, 129.09, 131.97, 133.00, 138.47, 142.52, 178.48 ppm. ESI-MS *m/z* (%): 400 (M + H, 100), 402 (M + H + 2, 96). Anal. calcd. for $C_{20}H_{22}BrN_3O$: C, 60.01; H, 5.54; N, 10.50. Found: C, 60.17; H, 5.64; N, 10.37.

*4.1.3.17. 1-benzyl-N′-(4-nitrobenzylidene)piperidine-4-carbohydrazide (**2g**).* Yield 86%; mp 219 °C. IR ν_{max}(cm^{-1}) 3185, 3078, 2947, 2917, 2803, 1672, 1614, 1601, 1583, 1515, 1390, 1336, 1230, 1109, 735, 695. ^{1}H NMR (400 MHz, $CDCl_3$) δ 1.88–1.94 (4H, m, piperidine-H), 2.14 (2H, t, J = 11.4 Hz, piperidine-H), 3.00 (2H, d, J = 11.8 Hz, piperidine-H), 3.17–3.21 (1H, m, piperidine-H), 3.56 (2H, s, N−CH_2), 7.26–7.38 (5H, m, H-2′, H-3′, H-4′, H-5′, H-6′), 7.79 (2H, d, J = 8.7 Hz, H-2″, H-6″), 7.81 (1H, s, N=CH), 8.27 (2H, d, J = 8.8 Hz, H-3″, H-5″), 9.47 (1H, bs, NH) ppm. ^{13}C NMR (100 MHz, $CDCl_3$) δ 27.99, 29.66, 38.72, 53.03, 63.26, 124.13, 127.02, 127.51, 128.20, 129.10, 139.78, 140.20, 144.93, 148.57, 177.82 ppm. ESI-MS *m/z* (%): 367 (M + H, 100). Anal. calcd. for $C_{20}H_{22}N_4O_3$: C, 65.56; H, 6.05; N, 15.29. Found: C, 65.69; H, 6.14; N, 14.92.

*4.1.3.18. 1-benzyl-N′-(4-cyanobenzylidene)piperidine-4-carbohydrazide (**2h**).* Yield 71%; mp 208 °C. IR ν_{max}(cm^{-1}) 3189, 3087, 3063, 2924, 2797, 2756, 2225, 1668, 1599, 1556, 1402, 1361, 1274, 1145, 737, 696. ^{1}H NMR (400 MHz, $CDCl_3$) δ 1.84–1.97 (4H, m, piperidine-H), 2.13 (2H, td, J = 3.1/11.2 Hz, piperidine-H), 3.00 (2H, d, J = 12.0 Hz, piperidine-H), 3.21 (1H, sept, J = 5.2 Hz, piperidine-H), 3.56 (2H, s, N−CH_2), 7.24–7.36 (5H, m, H-2′, H-3′, H-4′, H-5′, H-6′), 7.69 (2H, d, J = 8.0 Hz, H-2″, H-6″), 7.74 (2H, d, J = 8.0 Hz, H-3″, H-5″), 7.87 (1H, s, N=CH), 10.63 (1H, s, NH) ppm. ^{13}C NMR (100 MHz, $CDCl_3$) δ 28.06, 38.56, 53.09, 63.31, 113.06, 118.48, 127.01, 127.36, 128.19, 129.09, 132.52, 138.22, 138.30, 141.42, 178.67 ppm. ESI-MS *m/z* (%): 347 (M + H, 100). Anal. calcd. for $C_{21}H_{22}N_4O$: C, 72.81; H, 6.40; N, 16.17. Found: C, 72.68; H, 6.51; N, 16.16.

*4.1.3.19. 1-benzyl-N′-(4-(dimethylamino)benzylidene)piperidine-4-carbohydrazide (**2i**).* Yield 65%; mp 160 °C. IR ν_{max}(cm^{-1}) 3371, 3206, 3063, 3007, 2920, 2853, 2809, 1647, 1604, 1591, 1525, 1434, 1363, 1307, 1183, 1119, 804, 702. ^{1}H NMR (400 MHz, $CDCl_3$) δ 1.87–1.92 (5H, m, piperidine-H), 2.10–2.23 (3H, m, piperidine-H), 3.02 (6H, s, N−(CH_3)$_2$), 3.20 (1H, quin, J = 7.8 Hz, piperidine-H), 3.55 (2H, s, N−CH_2), 6.70 (2H, d, J = 8.8 Hz, H-3″, H-5″), 7.30–7.37 (5H, m, H-2′, H-3′, H-4′, H-5′, H-6′), 7.51 (2H, d, J = 8.8 Hz, H-2″, H-6″), 7.67 (1H, s, N=CH), 9.40 (1H, bs, NH) ppm. ^{13}C NMR (100 MHz, $CDCl_3$) δ 27.89, 38.55, 40.19, 53.22, 63.30, 111.86, 121.78, 126.93, 128.16, 128.40, 129.15, 138.39, 144.16, 151.60, 177.41 ppm. ESI-MS *m/z* (%): 365 (M +H, 100). Anal. calcd. for $C_{22}H_{28}N_4O$. 0.9 H_2O: C, 69.41; H, 7.89; N, 14.72. Found: C, 69.43; H, 7.85; N, 14.57.

*4.1.3.20. 1-benzyl-N′-(4-(diethylamino)benzylidene)piperidine-4-carbohydrazide (**2j**).* Yield 59%; mp 157 °C. IR ν_{max}(cm^{-1}) 3164, 3059, 2961, 2924, 2801, 1658, 1598, 1529, 1506, 1402, 1347, 1268, 1180, 1157, 820, 701. ^{1}H NMR (400 MHz, $CDCl_3$) δ 1.19 (6H, t, J = 7.0 Hz, N−($CH_2\underline{CH_3}$)$_2$), 1.87–1.93 (5H, m, piperidine-H), 2.10–2.16 (1H, m, piperidine-H), 2.98 (2H, d, J = 12.0 Hz, piperidine-H), 3.21 (1H, quin, J = 7.8 Hz, piperidine-H), 3.34–3.43 (4H, m, N−($\underline{CH_2}CH_3$)$_2$), 3.55 (2H, s, N−CH_2), 6.66 (2H, d, J = 8.0 Hz, H-3″, H-5″), 7.30–7.38 (5H, m, H-2′, H-3′, H-4′, H-5′, H-6′), 7.49 (2H, d, J = 8.0 Hz, H-2″, H-6″), 7.67 (1H, s, N=CH), 9.52 (1H, s, NH) ppm. ^{13}C NMR (100 MHz, $CDCl_3$) δ 12.58, 27.96, 38.61, 44.44, 53.29, 63.33, 111.25, 120.90, 126.87, 128.14, 128.66, 129.09, 138.61, 144.17, 148.84, 177.43 ppm. ESI-MS *m/z* (%): 393 (M+H, 100). Anal. calcd. for $C_{24}H_{32}N_4O$. 0.1 C_2H_5OH: C, 73.19; H, 8.27; N, 14.11. Found: C, 72.96; H, 7.91; N, 14.46.

4.2. Biological activity assays

4.2.1. Acetylcholinesterase/Butyrylcholinesterase activity

AChE (E.C. 3.1.1.7., Type VI-S, from electric eel and and recombinant human enzyme) and BuChE (E.C. 3.1.1.8, from equine serum and from human serum) were purchased from Sigma-Aldrich (St. Louis, MO, USA). 5,5′-Dithiobis(2-nitrobenzoic acid) (DTNB, Ellman's reagent), acetylthiocholine iodide (ATC), buffer compounds (potassium dihydrogen phosphate, potassium hydroxide) and sodium hydrogen carbonate were obtained from Fluka (Bachs, Switzerland). *S*-Butyrylthiocholine iodide (BTC) and DMSO were obtained from Sigma-Aldrich (St. Louis, MO, USA). Spectrophotometric measurements were performed on a Shimadzu 160-A UV–Vis spectrophotometer.

The inhibitory effects of the synthesized compounds on AChE and BuChE were evaluated using a slightly modified colorimetric method of Ellman et al. [27,28], with galantamine, rivastigmine and tacrine as the positive controls. Prior to use, all solutions were adjusted to 20 °C. Enzyme solution (100 μL) and inhibitor solution (100 μL) were added into a cuvette containing the phosphate buffer (3.0 mL, 0.1 M; pH 8.0). After 5 min incubation, required aliquots of the DTNB solution (100 μL) and of the ATC/BTC (20 μL) were added. After rapid and immediate mixing the absorption was measured at 412 nm by UV spectroscopy. As a reference, an identical solution of the enzyme without the inhibitor is processed following the same protocol. The blank reading contained 3.0 mL buffer, 200 μL water, 100 μL DTNB, and 20 μL substrate. The enzyme activity was determined in the presence of at least five different concentrations of an inhibitor, generally between 10^{-2} and 10^{-8}, in order to obtain inhibition of AChE or BuChE activity between 0 and 100%. Each concentration was assayed in triplicate. The samples were investigated immediately after preperation. The AChE/BuChE inhibitory activities and selectivity of piperidine compounds' results are summarized in Tables 1 and 2.

4.2.2. Kinetic studies of inhibition on AChE and BuChE

The kinetic study of AChE and BuChE were performed by Ellman's method [27,28] using *ee*AChE and *eq*BuChE. The reciprocal plots of the 1/V versus 1/[S] were obtained by various concentrations of ATC and BTC for compounds **1g** and **1j**, respectively. Linear regression was used for the calculation of Lineweaver-Burk plots. The increase of the absorbances were measured with different inhibitor concentrations (**1g**; 2.5, 5, 10, μM and **1j**; 1, 2, 4 μM) and without inhibitor. Seven different concentrations of substrate for both assays were set between 0.113 and 0.791 mM. Each experiment was performed in triplicate and all calculations were performed using SigmaPlot software (version 14.0).

4.2.3. Tioflavin T fluorescence assay ($A\beta_{42}$ aggregation assay)

Aβ-aggregation was determined using a Thioflavin T β-Amyloid (1–42) Aggregation Kit (AS-72214, SensoLyte®, AnaSpec) according to the manufacturer's protocol. Assays were performed on 96-well fluorescence microtiter plates (Nunc GmbH, Germany). Aβ peptide was diluted in 1 mL of cold assay buffer and sonicated for 5 min, followed by centrifugation at 10,000 rpm for 5 min at 4 °C. 10 μL of Thioflavin T solution (2 mM), 85 μL of the Aβ solution and 5 μL of the inhibitors (to reach final concentrations of 100 μM and 25 μM) or control were added into each well. The fluorescence emission was monitored at Ex/Em = 440/484 nm at 37 °C every 5 min for 180 min with 15 s shaking between reads using Thermo Scientific Varioskan Flash Spectrophotometer (Thermo Scientific, USA). Curcumin was used as the reference compound and the inhibitory results are summarized in Table 1.

4.2.4. Antioxidant activity

4.2.4.1. DPPH radical scavenging activity. Free radical scavenging activity of the compounds was evaluated by DPPH method using trolox as the reference standard [30]. The principle of the assay is the color change of DPPH solution from purple to yellow as the radical is quenched by antioxidants present in the sample [31]. The degree of discoloration of DPPH indicates the scavenging activity of the antioxidant regarding hydrogen donating ability. 1.5 mL compounds of the sample in methanol at different concentrations were mixed with 0.5 mL of freshly prepared 0.5 mM DPPH in methanol. The mixture was kept for 30 min in the dark at room temperature. The absorbance was measured at 517 nm against a blank (DPPH) on Thermo Scientific Varioskan® Flash microplate reader. The radical scavenging activity was measured as a decrease in the absorbance of DPPH. Each experiment was run in triplicate. The DPPH radical scavenging activity of the compounds was calculated according to the following equation [31]:

DPPH radical scavenging activity (%) = (A_{DPPH} − A_{sample})/(A_{DPPH}) × 100

4.2.4.2. ABTS radical cation scavenging activity. This method was based on the ability of different substances to scavenge 2,2′-azinobis-(3-ethylbenzothiazoline-6-sulfonic acid ($ABTS^+$) radical cation. The ability of the test sample to scavenge $ABTS^{\cdot+}$ radical cation was compared to trolox standard. The assay was performed according to an improved method as described by Re et al. [32] with some minor modification [33]. ABTS was dissolved in methanol to a 7 mM concentration. ABTS radical cation ($ABTS^{\cdot+}$) was produced by reacting ABTS stock solution with 2.45 mM potassium persulfate (1:1) and allowing the mixture to stand in the dark at room temperature for 12–16 h until the reaction was complete. The $ABTS^+$ solution was diluted with methanol to absorbance of 0.700 ± 0.05 at 734 nm for the method. 0.9 mL of ABTS radical cation solution was mixed with 0.1 mL of the test sample, and the absorbance was measured at 734 nm after 30 min. The absorbance was measured against a blank ($ABTS^+$) on Thermo Scientific Varioskan® Flash microplate reader. The radical scavenging activity was measured as a decrease in the absorbance of ABTS. Each experiment was run in triplicate.

ABTS cation radical scavenging activity (%) = [(A_{blank} − A_{sample})/A_{blank}] × 100

4.3. Molecular modeling studies

4.3.1. Docking studies

*4.3.1.1. Donepezil and compound **1g** in TcAChE.* First, the crystal structure of donepezil in complex with *Tc*AChE (PDB code 1EVE) resolved at 2.5 Å was downloaded from Protein Data Bank. After the water molecules were removed (except for the ones in the binding mode), the enzyme was protonated via protonate 3D protocol and subjected to energy minimization using AMBER99 force field in MOE2018.09 [36]. In order to validate the binding mode of donepezil and suggest a binding mode for the most active compound (**1g**) in *Tc*AChE, donepezil was taken from 1EVE crystal structure and compound **1g** was built in MOE2018.09. After the two molecules were protonated and energy minimized by using MMFF94x, docking simulations were carried out with GOLD 5.2 program with default settings [39]. The binding site was defined around the backbone carbon of His440 with a sphere of 22 Å. Goldscore standard precision was selected as the scoring function and 250 confirmations were allowed.

In terms of the validation of donepezil, the first ranked docking pose of donepezil inside the active gorge of *Tc*AChE enzyme with 2 water molecules was selected. The phenyl part of donepezil formed π-π interaction with Trp84 at the deep of the gorge while the other terminal with indanone moiety reached to Trp279 at PAS. Also, quaternary nitrogen atom of the piperidine ring and the side chain of Ser122 interacted through hydrogen bond at CAS region (Fig. 1).

The selected pose of compound **1g** reproduced a similar geometry as shown in Fig. 1 in the active gorge of *Tc*AChE. The benzyl part of the molecule reached to the deep of the gorge near Trp84 and the benzylidene part lied towards Trp279. Hydrazone nitrogen and the side chain of Tyr121 located at the middle of the gorge interacted through hydrogen bond. Also two hydrogen bonds were formed by the piperidine nitrogen; one of them as an intramolecular H-bond and the other one with one of the active water molecules.

*4.3.1.2. Compound **1j** in homology model BuChE.* The most active compound against *eq*BuChE (compound **1j**) was built, protonated and energy minimized by using MMFF94x. Homology model BuChE generated in one of our previous studies was used due to the lack of *eq*BuChE crystal structure [40]. A sphere of 20 Å around the backbone carbon of His438 was defined as the binding site and 250 confirmations were allowed with Goldscore and Chemscore scoring functions.

The proposed binding mode of compound **1j** in BuChE demonstrated key interactions. NH group of the hydrazide-hydrazone part interacted with Ala328 through hydrogen bond at the middle of the gorge. Also, piperidine N formed a hydrogen bond with His438 near the deep of the gorge and a π-π interaction might be speculated between Trp82 and benzyl part at the deep of the gorge (Fig. 3).

4.3.1.3. Compound 2g in huAChE and compound 1a in huBuChE. The cyrstal structure of donepezil in complex with *hu*AChE (PDB code: 4EY7, 2.35A resolution) and the cyrstal structure of *hu*BuChE (PDB code: 2PM8, 2.8 Å resolution) were taken from Protein Data Bank. Water molecules were removed (except for the one conserved in the active site for 4EY7), the enzyme was protonated and energy minimized using AMBER99 forcefield. Compound **2g** and compound **1a** were builded, protonated and energy minimized by using MMFF94x forcefield in MOE2018.09. Docking simulations were carried out with GOLD 5.2 program with default settings. The binding site was defined around the backbone carbon of His447 with a sphere of 20 Å using Goldscore standard precision for Compound **2g** in *hu*AChE and around the backbone carbon of His438 with a sphere of 22 Å using Chemscore standard precision for Compound **1a** in *hu*BuChE. 100 confirmations were allowed for both docking studies.

The proposed binding mode of compound **2g** inside the active gorge of *hu*AChE has a π-π interaction between phenyl group and Trp86 and a cation-π interaction between the protonated nitrogen and the phenyl group of Tyr341 (Fig. 2).

The proposed binding interactions of compound **1a** in complex with *hu*BuChE are a cation-π interaction between the protonated nitrogen and the phenyl group of Trp82 and a π-π interaction between phenyl group and Tyr332 (Fig. 4).

4.3.2. Molecular dynamics simulations

Molecular dynamics simulations were carried out for the selected poses of donepezil and compound **1g** in complex with *Tc*AChE, compound **2g** in complex with *hu*AChE and also for compound **1j** in complex with model BuChE. AMBER 14 program was used for all the preparation steps of the complexes and AMBER 12 program was used for the simulation part [41].

After the atom types and the partial charges of donepezil, compound **1g,** compound **2g** and compound **1j** with selected geometries were added by antechamber module, the compounds were parameterized with *Gaff* force field using parmchk module [42]. Then, *Tc*AChE, *hu*AChE and model BuChE were protonated and parameterized by ff99SB force field [41]. The complexes were created by Leap module of AMBER. Donepezil-*Tc*AChE, compound **1g**-*Tc*AChE, compound **2g**-*hu*AChE and compound **1j**-model BuChE complexes were neutralized by 9 K^+, 9Na^+, 9Na^+ and 6Cl^- counterions, respectively. The complexes were solvated by ~14,569, ~14,561, ~14,550 and ~14,447 water molecules for each complex, respectively, in octahedral box using TIP3P leaving at least 10 Å between the solute atoms and the border of the box [43]. The solvated and neutralized complexes were energy minimized by Sander module of AMBER. Then, the systems were heated from 50 to 300 K with positional restrains (force constant: 10 kcal/mol/Å) for 300 ps allowing the solvent and the counterions to move freely. 9 Å cutoff for the short-range nonbonded interactions was used combined with the particle mesh Ewald option [44]. In order to constrain bond vibrations involving the hydrogen atoms, Settle algorithm was used [45]. During the fallowing 300 ps, the positional restrains were reduced to allow unrestrained MD simulations for all atoms over the equilibration time of 2 ns. Further 80 ns free MD simulations were performed using these equilibrated structures as starting complexes. VMD was used for the visualization of the trajectories and XMGRACE software was used for preparing the plots [46,47].

The molecular dynamics simulation of donepezil inside *Tc*AChE with the selected geometry were stable throughout the whole 80 ns simulation. The phenyl part of donepezil was the only part that changed the RMSD value. At the beginning, the whole geometry was conserved for ~20 ns, then the average root mean square deviation (RMSD) increased from 2 Å up to 3.2 Å and the phenyl part of the ligand lost the π-π interaction for ~35 ns and leaned up to Ser122 at 55th ns with a RMSD value of 5 Å without losing the key interaction. After the 55th ns, the ligand started to get back at the initial geometry and after 75 ns, the starting geometry was observed again and was conserved till the end of the simulation. The average RMSD value of the protein is ~2.07 Å for the whole MD (Fig. S1).

In case of compound **1g** inside *Tc*AChE, the ligand was stable during the 80 ns simulation and the key interactions in the initial structure were generally conserved throughout the simulation except for the one with the selected water molecule. At the beginning, the average RMSD value of the ligand compared to the initial structure was ~3.2 Å due to a rearrangement of the structure inside the enzyme without losing the key hydrogen bond interaction but then the ligand kept stable for the whole simulation. The average RMSD value of the protein was ~1.98 Å for the whole MD (Fig. S1).

On the other hand, compound **2g** inside *hu*AChE was also stable for

the whole 80 ns simulation, but changed the geometry by changing the position of the phenyl moiety and by losing the π-π interaction of compound **1g** at the beginning without losing the cation-π interaction. The RMSD value of the ligand reached up to 4.5 Å during the first 7 ns but kept stable afterwards. The average RMSD of the ligand was 2.857 while the average RMSD value of the protein was ~1.56 Å for the whole 80 ns MD (Fig. S2).

Regarding compound **1j** inside model BuChE, the binding mode of compound **1j** demonstrated stability inside for the 80 ns MD simulation. The average RMSD of the ligand reached up to 3.3 Å in the first part of the MD without losing the key interactions except for the π-π interaction of the benzyl group with Trp82. After the first ~3 ns, the benzyl group formed π-π interaction with Trp82 again until the ~65th ns where the benzyl group rearranged itself and moved back to its starting geometry after 70th ns till the end of the MD. The average RMSD value of the protein reached its steady state around ~1.80 Å with a slight change of its geometry during the 80 ns MD (Fig. S3).

Acknowledgements

This project was supported by TUBITAK (The Scientific and Technological Research Council of Turkey), Project Number: 214S083.

Conflict of interest

The authors report no conflict of interests.

Appendix A. Supplementary material

Supplementary data to this article can be found online at https://doi.org/10.1016/j.bioorg.2018.11.051.

References

[1] https://www.alz.co.uk/research/WorldAlzheimerReport2016.pdf.
[2] P. Davies, J.F. Maloney, Selective loss of central cholinergic neurons in Alzheimer's disease, Lancet 308 (1976) 1403.
[3] J. Hardy, D. Allsop, Amyloid deposition as the central event in the aetiology of Alzheimer's disease, Trends Pharmacol. Sci. 12 (1991) 383–388.
[4] A.C. Alonso, I. Grundke-Iqbal, K. Iqbal, Alzheimer's disease hyperphosphorylated tau sequesters normal tau into tangles of filaments and disassembles microtubules, Nat. Med. 2 (1996) 783–787.
[5] A. Tramutola, C. Lanzillotta, M. Perluigi, D.A. Butterfield, Oxidative stress, protein modification and Alzheimer disease, Brain Res. Bull. 133 (2017) 88–96.
[6] D. Muñoz-Torrero, Acetylcholinesterase inhibitors as disease-modifying therapies for Alzheimer's disease, Curr. Med. Chem. 15 (2008) 2433–2455.
[7] M.M. Mesulam, A. Guillozet, P. Shaw, A. Levey, E.G. Duysen, O. Lockridge, Acetylcholinesterase knockouts establish central cholinergic pathways and can use butyrylcholinesterase to hydrolyze acetylcholine, Neuroscience 110 (2002) 627–639.
[8] N.H. Greig, T. Utsuki, Q. Yu, X. Zhu, H.W. Holloway, T. Perry, B. Lee, D.K. Ingram, D.K. Lahiri, A new therapeutic target in Alzheimer's disease treatment: attention to butyrylcholinesterase, Curr. Med. Res. Opin. 17 (2001) 159–165.
[9] I.W. Hamley, Peptide fibrillization, Angew. Chem. Int. Ed. Engl. 46 (2007) 8128–8147.
[10] N.C. Inestrosa, A. Alvarez, C.A. Perez, R.D. Moreno, M. Vicente, C. Linker, O.I. Casanueva, C. Soto, J. Garrido, Acetylcholinesterase accelerates assembly of amyloid-beta-peptides into Alzheimer's fibrils: possible role of the peripheral site of the enzyme, Neuron. 16 (1996) 881–891.
[11] J.L. Sussman, M. Harel, F. Frolow, C. Oefner, A. Goldman, L. Toker, I. Silman, Atomic structure of acetylcholinesterase from Torpedo californica: a prototypic acetylcholine-binding protein, Science 253 (1991) 872–879.
[12] M. Rosini, E. Simoni, M. Bartolini, A. Cavalli, L. Ceccarini, N. Pascu, D.W. McClymont, A. Tarozzi, M.L. Bolognesi, A. Minarini, V. Tumiatti, V. Andrisano, I.R. Mellor, C. Melchiorre, Inhibition of acetylcholinesterase, beta-amyloid aggregation, and NMDA receptors in Alzheimer's disease: a promising direction for the multi-target-directed ligands gold rush, J. Med. Chem. 51 (2008) 4381–4384.
[13] D. Alonso, I. Dorronsoro, L. Rubio, P. Muñoz, E. Garcia-Palomero, M. Del Monte, A. Bidon-Chanal, M. Orozco, F.J. Luque, A. Castro, M. Medina, A. Martinez, Donepezil-tacrine hybrid related derivatives as new dual binding site inhibitors of AChE, Bioorg. Med. Chem. 13 (2005) 6588–6597.
[14] L. Piazzi, F. Belluti, A. Bisi, S. Gobbi, S. Rizzo, M. Bartolini, V. Andrisano, M. Recanatini, A. Rampa, Cholinesterase inhibitors: SAR and enzyme inhibitory activity of 3-[ω-(benzylmethylamino)alkoxy]xanthen-9-ones, Bioorg. Med. Chem. 15 (2007) 575–585.
[15] D.A. Butterfield, J. Drake, C. Pocernich, A. Castegna, Evidence of oxidative damage in Alzheimer's disease brain: central role for amyloid beta-peptide, Trends Mol. Med. 7 (2001) 548–554.
[16] M.A. Smith, G. Perry, W.A. Pryor, Causes and consequences of oxidative stress in Alzheimer's disease, Free Radic. Biol. Med. 32 (2002) 1049.
[17] Q. Liu, F. Xie, R. Rolston, P.I. Moreira, A. Nunomura, X. Zhu, M.A. Smith, G. Perry, Prevention and treatment of Alzheimer disease and aging: antioxidants, Mini-Rev. Med. Chem. 7 (2007) 171–180.
[18] D. Pratico, Oxidative stress hypothesis in Alzheimer's disease: a reappraisal, Trends Pharmacol. Sci. 29 (2008) 609–615.
[19] P.C. Trippier, K. Jansen Labby, D.D. Hawker, J.J. Mataka, R.B. Silverman, Target- and mechanism-based therapeutics for neurodegenerative diseases: strength in numbers, J. Med. Chem. 56 (2013) 3121–3147.
[20] F.M. Longo, S.M. Massa, Neuroprotective strategies in Alzheimer's disease, NeuroRx 1 (2004) 117–127.
[21] M.I. Fernandez-Bachiller, C. Perez, L. Monjas, J. Rademann, M.I. Rodriguez-Franco, New tacrine-4-oxo-4H-chromene hybrids as multifunctional agents for the treatment of Alzheimer's disease, with cholinergic, antioxidant, and β-amyloid-reducing properties, J. Med. Chem. 55 (2012) 1303–1317.
[22] L.M. Refolo, H.M. Fillit, Drug discovery for Alzheimer's disease: the end of the beginning, J. Mol. Neurosci. 24 (2004) 1–8.
[23] A.S. Alpan, S. Parlar, L. Carlino, A.H. Tarikogullari, V. Alptüzün, H.S. Güneş, Synthesis, biological activity and molecular modeling studies on 1*H*-benzimidazole derivatives as acetylcholinesterase inhibitors, Bioorg. Med. Chem. 21 (2013) 4928–4937.
[24] S. Bala, G. Uppal, S. Kamboj, V. Saini, D.N. Prasad, Design, characterization, computational studies, and pharmacological evaluation of substituted-*N*′-[(1E) substituted-phenylmethylidene]benzohydrazide analogs, Med. Chem. Res. 22 (2012) 2755–2767.
[25] R.M. Silverstein, G.C. Bassler, T.C. Morrill, Spectrometric Identification of Organic Compounds, John Wiley & Sons, New York, 1981 Chapter 3.
[26] V. Sridharan, S. Saravanan, S. Muthusubramanian, S. Sivasubramanian, NMR investigation of hydrogen bonding and 1,3-tautomerism in 2-(2-hydroxy-5-substituted-aryl) benzimidazoles, Magn. Reson. Chem. 43 (2005) 551–556.
[27] G.L. Ellman, K.D. Courtney, V. Andres Jr, R.M. Featherstone, A new and rapid colorimetric determination of acetylcholinesterase activity, Biochem. Pharmacol. 7 (1961) 88–95.
[28] P. Kapková, N. Stiefl, U. Sürig, B. Engels, K. Baumann, U. Holzgrabe, Synthesis, biological activity, and docking studies of new acetylcholinesterase inhibitors of the bispyridinium type, Arch. Pharm. Pharm. Med. Chem 336 (2003) 523–540.
[29] H. Levine, Thioflavine T interaction with synthetic Alzheimer's disease beta-amyloid peptides: detection of amyloid aggregation in solution, Protein Sci. 2 (1993) 404–410.
[30] C.H. Yang, R.X. Li, L.Y. Chuang, Antioxidant activity of various parts of Cinnamomum cassia extracted with different extraction methods, Molecules 17 (2012) 7294–7304.
[31] V.G. Kamleshiya, A.H. Meshram, Ansari, Comparative evaluation of antioxidant and free-radical scavenging activity of aqueous and methanolic spice extracts, Int. J. Life Sci. Pharm. Res. 2 (2012) 118–125.
[32] R. Re, N. Pellegrini, A. Proteggente, A. Pannala, M. Yang, C. Rice-Evans, Antioxidant activity applying an improved ABTS radical cation decolorization assay, Free Radic. Biol. Med. 26 (1999) 1231–1237.
[33] E.A. Shalaby, S.M.M. Shanab, Comparison of DPPH and ABTS assays for determining antioxidant potential of water and methanol extracts of Spirulina platensis, Indian J. Geo-Mar. Sci. 42 (2013) 556–564.
[34] C. Galdeano, E. Viayna, P. Arroyo, A. Bidon-Chanal, J.R. Blas, D. Munoz-Torrero, F.J. Luque, Structural determinants of the multifunctional profile of dual binding site acetylcholinesterase inhibitors as anti-Alzheimer agents, Curr. Pharm. Des. 16 (2010) 2818–2836.
[35] H. Lineweaver, D. Burk, The determination of enzyme dissociation constants, J. Am. Chem. Soc. 56 (1934) 658–666.
[36] Molecular Operating Environment (MOE), 2013.08; Chemical Computing Group ULC, 1010 Sherbooke St. West, Suite #910, Montreal, QC, Canada, H3A 2R7, 2018.
[37] H. Pajouhesh, G.R. Lenz, Medicinal chemical properties of successful central nervous system drug, NeuroRx 2 (2005) 541–553.
[38] Z. Rankovic, CNS drug design: balancing physicochemical properties for optimal brain exposure, J. Med. Chem. 58 (2015) 2584–2608.
[39] G. Jones, P. Willett, R.C. Glen, A.R. Leach, R. Taylor, Development and validation of a genetic algorithm for flexible docking, J. Mol. Biol. 267 (1997) 727–748.
[40] G. Coban, L. Carlino, A.H. Tarikogullari, S. Parlar, G. Sarıkaya, V. Alptüzün, A.S. Alpan, H.S. Güneş, E. Erciyas, 1*H*-benzimidazole derivatives as butyrylcholinesterase inhibitors: synthesis and molecular modeling studies, Med. Chem. Res. 25 (2016) 2005–2014.
[41] D.A. Case, T.A. Darden, T.E. Cheatham, C.L. Simmerling, J. Wang, R.E. Duke, R. Luo, R.C. Walker, W. Zhang, K.M. Merz, B. Roberts, S. Hayik, A. Roitberg, G. Seabra, J. Swails, A.W. Goetz, I. Kolossváry, K.F. Wong, F. Paesani, J. Vanicek, R.M. Wolf, J. Liu, X. Wu, S.R. Brozell, T. Steinbrecher, H. Gohlke, Q. Cai, X. Ye, J. Wang, M.J.

Hsieh, G. Cui, D.R. Roe, D.H. Mathews, M.G. Seetin, R. Salomon-Ferrer, C. Sagui, V. Babin, T. Luchko, S. Gusarov, A. Kovalenko, P.A. Kollman, Amber 12, 2012.
[42] J. Wang, R.M. Wolf, J.W. Caldwell, P.A. Kollman, D.A. Case, Development and testing of a general amber force field, J. Comput. Chem. 25 (2004) 1157–1174.
[43] W. Jorgensen, J. Chendrasekhar, J.D. Madura, R.W. Impey, M.L. Klein, Comparison of simple potential functions for simulating liquid water, J. Chem. Phys. 79 (79) (1983) 926–935.
[44] U. Essmann, L. Petera, M.L. Berkowitz, T. Darden, H. Lee, L.G. Pedersen, A smooth particle mesh ewald method, J. Chem. Phys. 103 (1995) 8577–8593.
[45] S. Miyamoto, P.A. Kollmann, Settle: an analytical version of the SHAKE and RATTLE algorithm for rigid water models, J. Comput. Chem. 13 (1992) 952–962.
[46] W. Humphrey, A. Dalke, K. Schulten, VMD: visual molecular dynamics, J. Mol. Graph. 14 (1996) 27–28.
[47] P.J. Turner, XMGRACE, Version 5.1.25-5. Center for Coastal and Land-Margin Research, Oregon Graduate Institute of Science and Technology, Beaverton, OR, 2005.